

SimMC: Simple Masked Contrastive Learning of Skeleton Representations for Unsupervised Person Re-Identification

Haocong Rao and Chunyan Miao[†]

School of Computer Science and Engineering, Nanyang Technological University
Joint NTU-UBC Research Centre of Excellence in Active Living for the Elderly (LILY)
haocong001@ntu.edu.sg, ascymiao@ntu.edu.sg

Abstract

Recent advances in skeleton-based person re-identification (re-ID) obtain impressive performance via either hand-crafted skeleton descriptors or skeleton representation learning with deep learning paradigms. However, they typically require skeletal pre-modeling and label information for training, which leads to limited applicability of these methods. In this paper, we focus on *unsupervised* skeleton-based person re-ID, and present a generic Simple Masked Contrastive learning (SimMC) framework to learn effective representations from *unlabeled* 3D skeletons for person re-ID. Specifically, to fully exploit skeleton features within each skeleton sequence, we first devise a *masked prototype contrastive learning (MPC)* scheme to cluster the most typical skeleton features (*skeleton prototypes*) from different subsequences randomly masked from raw sequences, and contrast the inherent similarity between skeleton features and different prototypes to learn discriminative skeleton representations without using any label. Then, considering that different subsequences within the same sequence usually enjoy strong correlations due to the nature of motion continuity, we propose the *masked intra-sequence contrastive learning (MIC)* to capture intra-sequence pattern consistency between subsequences, so as to encourage learning more effective skeleton representations for person re-ID. Extensive experiments validate that the proposed SimMC outperforms most state-of-the-art skeleton-based methods. We further show its scalability and efficiency in enhancing the performance of existing models*.

1 Introduction

Person re-identification (re-ID) targets at retrieving and matching the same pedestrian from different views or occasions, which assumes a pivotal role in various applications

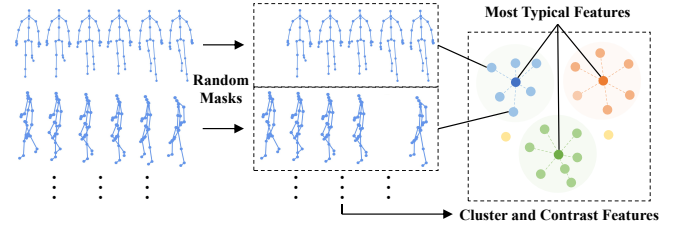


Figure 1: Our framework clusters the randomly masked skeleton sequences, and contrasts their features with the most typical ones to learn discriminative skeleton representations for person re-ID.

such as intelligent surveillance, robotics, and security authentication [Ye *et al.*, 2021]. Recently, person re-ID via 3D skeletons has drawn growing interests from academia and industry [Pala *et al.*, 2019; Rao *et al.*, 2021b; Rao *et al.*, 2021d]. Compared with conventional image-based methods that typically rely on visual features such as human silhouettes and appearances for recognition [Liu *et al.*, 2015], skeleton-based methods leverage 3D positions of key body joints to characterize discriminative structural and motion features of human body, which could enjoy smaller data size and better robustness against scale and view variation [Han *et al.*, 2017].

Despite the great progress in skeleton-based person re-ID, existing endeavors require either extracting hand-crafted features (*e.g.*, anthropometric attributes) [Pala *et al.*, 2019] or learning skeleton representations with the supervision of labels. For hand-crafted methods, they typically require extensive domain knowledge while lacking the flexibility to explore latent features beyond human cognition. To tackle this issue, numerous recent works resort to convolutional neural networks (CNN) [Liao *et al.*, 2020] and long short-term memory (LSTM) [Rao *et al.*, 2021a] to perform supervised or self-supervised skeleton representation learning. However, these methods usually require a specific pre-modeling of 3D skeletons (*e.g.*, skeleton graphs [Rao *et al.*, 2021d]), and rely on massive manually-annotated data to train or fine-tune models, which is labor-expensive and unable to learn general pedestrian representations under the unavailability of labels.

To address these challenges, this paper presents a generic Simple Masked Contrastive learning (SimMC) framework, as shown in Fig. 1, which contrasts the typical features and inherent relationships of *masked* skeleton sequences to learn

[†]Corresponding author

*Our codes are available at <https://github.com/Kali-Hac/SimMC>.

effective skeleton representations *without using any label* for person re-ID. Specifically, to fully utilize unique features within skeleton sequences, we first devise a **masked prototype contrastive learning (MPC)** scheme to cluster *subsequence* representations (referred as *skeleton instances*) randomly masked from raw sequences, and contrast the inherent similarity between them and the most typical features (referred as *skeleton prototypes*) to learn discriminative skeleton representations. By pulling closer skeleton instances belonging to the same prototype and pushing apart instances of different prototypes with the instance-prototype contrastive learning, MPC enables the model to capture discriminative skeleton features and high-level semantics (*e.g.*, intra-class skeleton similarity) from *unlabeled* skeleton sequences for the person re-ID task. Then, motivated by the nature of motion continuity that typically endows different subsequences with strong correlations (*e.g.*, motion similarity), we propose the **masked intra-sequence contrastive learning (MIC)** to learn the intra-sequence similarity between subsequences of the same skeleton sequence, which encourages capturing the pattern consistency within sequences to learn more effective representations of skeletons for person re-ID.

The proposed SimMC framework enjoys merits in terms of architectures, performance, and scalability. Firstly, SimMC is primarily built by multi-layer perceptron (MLP) networks with small model complexity, which can directly learn effective representations from raw skeleton sequences without any prior modeling. Secondly, the proposed unsupervised framework outperforms most existing self-supervised and supervised skeleton-based methods that utilize extra label information, and can also be efficiently applied to 3D skeleton data estimated from RGB-based scenes. Lastly, our framework can serve as a generic contrastive learning paradigm to fine-tune skeleton features learned from existing models, which benefits learning better skeleton representations for the task of person re-ID. In summary, our main contributions include:

- We present a simple masked contrastive learning (SimMC) framework that exploits typical features and relationships of masked unlabeled skeleton sequences to learn discriminative representations for person re-ID.
- We devise a novel masked prototype contrastive learning (MPC) scheme to fully contrast most representative features and learn high-level semantics from subsequence representations masked from skeleton sequences.
- We propose the masked intra-sequence contrastive learning (MIC) to learn inherent similarity and pattern consistency between subsequences, so as to encourage learning more effective representations for person re-ID.
- Empirical evaluations show that SimMC significantly outperforms most state-of-the-art skeleton-based methods on four benchmark datasets, and can be exploited to fine-tune existing skeleton representations and boost their performance with up to 28.2% mAP gains.

2 Related Works

Skeleton-based Person Re-identification. Most existing methods typically extract hand-crafted anthropometric, mor-

phological, and gait descriptors from 3D skeletons to characterize human body and motion features. Seven Euclidean distances between certain joints are utilized by [Barbosa *et al.*, 2012] to construct a distance matrix for person re-ID. Further enhancement with 13 (D_{13}) and 16 skeleton descriptors (D_{16}) are made in [Munaro *et al.*, 2014a] and [Pala *et al.*, 2019], respectively, which leverage k -nearest neighbor, support vector machine or Adaboost classifiers to perform person re-ID. Recently, deep neural networks are widely applied to supervised and self-supervised skeleton representation learning. A CNN-based paradigm, PoseGait [Liao *et al.*, 2020], is devised to encode 81 hand-crafted skeleton/pose features for human recognition. An LSTM-based skeleton encoding model with locality-aware attention (AGE) [Rao *et al.*, 2020] is proposed to learn discriminative gait features from skeleton sequences. SGELA [Rao *et al.*, 2021b] further combines multiple self-supervised pretext tasks (*e.g.*, reverse sequential reconstruction) and inter-sequence contrastive scheme to enhance skeleton pattern learning for person re-ID. The graph-based methods MG-SCR [Rao *et al.*, 2021d] and SM-SGE [Rao *et al.*, 2021a] devise multi-level skeleton graphs and auxiliary self-supervised tasks for person re-ID tasks.

Contrastive Learning. Contrastive learning is widely applied to various self-supervised and unsupervised paradigms [He *et al.*, 2020; Rao *et al.*, 2021b; Rao *et al.*, 2021c; Chen and He, 2021] to learn effective data representations by pulling together positive representation pairs and pushing apart negative ones in a certain feature space. An instance discrimination paradigm based on exemplar tasks [Wu *et al.*, 2018] is devised for image contrastive learning. The contrastive predictive coding (CPC) model with the probabilistic InfoNCE loss [Oord *et al.*, 2018] is proposed to learn general representations from various domains. Recent contrastive paradigms explore mini-batch negative sampling [Chen *et al.*, 2020] and momentum-based encoders [He *et al.*, 2020], while [Chen and He, 2021] devises a Siamese architecture for contrastive learning without using negative pairs or momentum encoders. In [Li *et al.*, 2021], contrastive learning and k -means clustering are combined for unsupervised learning of visual representations.

3 The Proposed Framework

Suppose that a 3D skeleton sequence $\mathcal{S}_{1:f} = (\mathcal{S}_1, \dots, \mathcal{S}_f) \in \mathbb{R}^{f \times K}$, where $\mathcal{S}_t \in \mathbb{R}^K$ is the t^{th} skeleton with 3D coordinates of J body joints and $K = J \times 3$. Each skeleton sequence $\mathcal{S}_{1:f}$ belongs to an identity y , where $y \in \{1, \dots, I\}$ and I is the number of different identities. The training set $\Phi_{\mathcal{T}} = \{\mathcal{S}_{1:f}^{\mathcal{T},i}\}_{i=1}^{N_1}$, probe set $\Phi_{\mathcal{P}} = \{\mathcal{S}_{1:f}^{\mathcal{P},i}\}_{i=1}^{N_2}$, and gallery set $\Phi_{\mathcal{G}} = \{\mathcal{S}_{1:f}^{\mathcal{G},i}\}_{i=1}^{N_3}$ contain N_1 , N_2 , and N_3 skeleton sequences of different persons in different views and scenes. Our framework aims at learning an encoder (denoted as $\psi(\cdot)$) built with neural networks to encode $\Phi_{\mathcal{P}}$ and $\Phi_{\mathcal{G}}$ into effective skeleton representations $\{v_i^{\mathcal{P}}\}_{i=1}^{N_2}$ and $\{v_j^{\mathcal{G}}\}_{j=1}^{N_3}$ *without using any label*, such that the representation $v_i^{\mathcal{P}}$ in probe set can match the representation $v_j^{\mathcal{G}}$ of the same identity in gallery set. The overview of our framework is presented in Fig. 2.

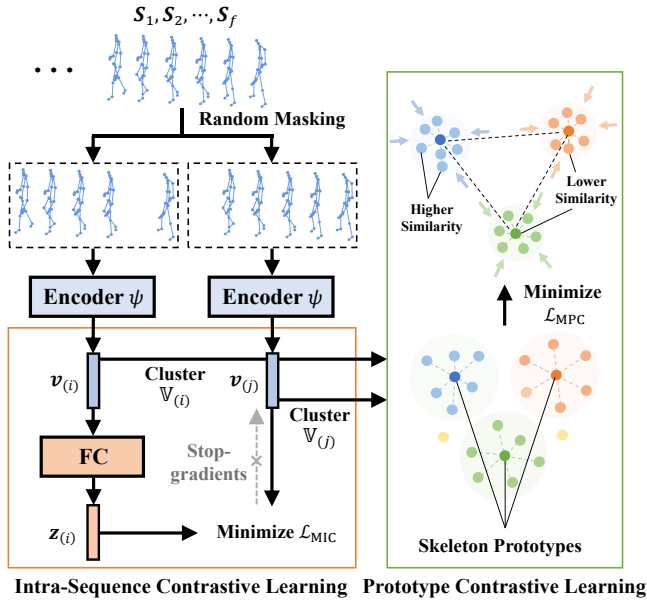


Figure 2: Schematics of our framework with masked prototype contrastive learning and masked intra-sequence contrastive learning.

As shown in Fig. 2, we firstly randomly mask each input skeleton sequence to sample i^{th} and j^{th} subsequences, which are encoded into skeleton instances $v_{(i)}$ and $v_{(j)}$ (see Sec. 3.1). Secondly, we cluster corresponding instance sets $\mathbb{V}_{(i)}$ and $\mathbb{V}_{(j)}$ individually to generate skeleton prototypes, and then enhance the similarity between instances of same prototype while maximizing the dissimilarity between different ones by minimizing \mathcal{L}_{MPC} . Meanwhile, a Siamese architecture is exploited to learn inherent intra-sequence similarity between $v_{(i)}$ and $v_{(j)}$ by minimizing \mathcal{L}_{MIC} (see Sec. 3.2).

3.1 Masked Prototype Contrastive Learning

Each person’s skeletons typically possess unique features (e.g., anthropometric attributes), while their corresponding sequences could carry recognizable and highly consistent walking patterns [Murray *et al.*, 1964]. Naturally, we expect the model to exploit the most representative skeleton patterns and traits *within each sequence* for person re-ID. A naïve solution is to cluster skeleton sequences to learn the representative features by direct inter-sequence contrastive learning, while it could overlook some valuable *intra-sequence* representations (e.g., subsequences) that might contain key patterns. To encourage the model to fully mine intra-sequence skeleton features and high-level semantics (e.g., identity-related patterns) from skeleton sequences, we propose a **masked prototype contrastive learning (MPC) scheme** to jointly focus on the most typical features (**skeleton prototypes**) of different subsequence representations (**skeleton instances**) randomly masked from original sequences, and exploit the instance-prototype similarity and dissimilarity to learn discriminative skeleton representations.

Given an input skeleton sequence $S_{1:f} = (S_1, \dots, S_f)$, we exploit an MLP encoder with one hidden layer to encode

each skeleton as:

$$h_j = \psi(S_j) = \mathbf{W}^2 \sigma(\mathbf{W}^1 S_j), \quad (1)$$

where $\psi(\cdot)$ represents the encoder function, $\mathbf{W}^1 \in \mathbb{R}^{H \times K}$ and $\mathbf{W}^2 \in \mathbb{R}^{H \times H}$ denote the learnable weight matrices to encode the j^{th} skeleton $S_j \in \mathbb{R}^K$ into a latent feature representation $h_j \in \mathbb{R}^H$, and $\sigma(\cdot)$ is a ReLU non-linear activation function. Then, to sample subsequence representations from the encoded sequence representation (h_1, \dots, h_f) of $S_{1:f}$, we utilize a masking function \mathcal{M} to randomly produce x masks, i.e., zero-masking positions, for each skeleton sequence of length f with:

$$\mathcal{M}(f, x) = (m_1, \dots, m_f), \quad (2)$$

where $m_j \in \{0, 1\}$ is the mask status for the j^{th} position of a sequence and $\sum_{j=1}^f m_j = f - x$. We apply the generated random masks to $S_{1:f}$ and its corresponding skeleton representations (h_1, \dots, h_f) (see Eq. (1)), which are then integrated into a subsequence representation as (see Fig. 2):

$$v_{(i)} = \frac{1}{f - x} \sum_{j=1}^f m_{(i),j} w_j h_j, \quad (3)$$

where $v_{(i)} \in \mathbb{R}^H$ ($i \in \{1, \dots, q\}$) denotes the feature representation of i^{th} subsequence sampled from $S_{1:f}$ using x random masks, q is the number of subsequence sampling, $m_{(i),j}$ denotes the mask status of the j^{th} position at the i^{th} sampling, while w_j represents the importance of j^{th} skeleton representation h_j . Here each skeleton is assumed to equally contribute to representing sequence features, i.e., $w_j = 1$. For clarity, we use $\mathbb{V}_{(i)} = \{v_{(i),j}\}_{j=1}^{N_1}$ to denote all subsequence representations in the i^{th} subsequence sampling of the training set $\Phi_{\mathcal{T}}$. Note that we sample one random subsequence for each training sequence at each sampling. $\mathbb{V}_{(i)} = \{v_{(i),j}\}_{j=1}^{N_1}$ are exploited as *skeleton instances* for the MPC scheme.

To group feature-similar skeleton instances and discover semantic clusters with arbitrary shapes, we leverage the DBSCAN algorithm [Ester *et al.*, 1996] to perform clustering *individually* on the i^{th} instance set $\mathbb{V}_{(i)}$ corresponding to i^{th} subsequence sampling, as shown in Fig. 2, and generate clusters $\bar{\mathbb{V}}_{(i)}^c = \{v_{(i),j}^c\}_{j=1}^{N_c}$, $c \in \{1, \dots, C\}$, where C is the number of clusters (i.e., pseudo classes), and each cluster $\bar{\mathbb{V}}_{(i)}^c$ contains N_c instances belonging to the c^{th} pseudo class. We *averagely aggregate* instance features of the same cluster to generate the corresponding skeleton prototype as:

$$p_{(i)}^c = \frac{1}{N_c} \sum_{j=1}^{N_c} v_{(i),j}^c, \quad (4)$$

where $p_{(i)}^c \in \mathbb{R}^H$ denotes the skeleton prototype of the c^{th} cluster $\bar{\mathbb{V}}_{(i)}^c$. To jointly focus on the representative skeleton features in all instance sets and encourage capturing high-level skeleton semantics from different prototypes, we exploit a masked prototype contrastive (MPC) loss to enhance the

similarity of each skeleton instance to the corresponding prototype and maximize its dissimilarity to other prototypes by:

$$\mathcal{L}_{\text{MPC}} = \frac{1}{N} \sum_{i=1}^q \sum_{c=1}^{C_i} \sum_{j=1}^{N_c} -\log \frac{\exp(\mathbf{v}_{(i),j}^c \cdot \mathbf{p}_{(i)}^c / \tau)}{\sum_{k=1}^{C_i} \exp(\mathbf{v}_{(i),j}^c \cdot \mathbf{p}_{(i)}^k / \tau)}, \quad (5)$$

where N represents the number of all skeleton instances, C_i denotes the number of skeleton prototypes generated from the i^{th} instance set $\mathbb{V}_{(i)}$, N_c is the number of instances belonging to the c^{th} prototype $\mathbf{p}_{(i)}^c$ in $\mathbb{V}_{(i)}$, and τ represents the temperature for contrastive learning. It is worth noting that the naïve prototype contrastive learning (denoted as NPC) using original sequences is a special case of the proposed MPC scheme when $q = 1$ and $x = 0$ (see Eq. (2) and (3)). The MPC scheme can be viewed as to perform finer prototype learning with different subsequences, and allow the model to jointly attend to key skeleton patterns from different representation subspaces of the original sequences, which encourages capturing more discriminative skeleton features for person re-ID (see Sec. 5). The objective of MPC can be theoretically formulated in the form of Expectation-Maximization (EM) algorithms. We prove the effectiveness of MPC and show its relations to existing contrastive losses in Appendix A.

3.2 Masked Intra-Sequence Contrastive Learning

The continuity of human motion typically results in very little variation of poses/skeletons within a small temporal interval [Rao *et al.*, 2021b]. Due to this nature, subsequences of the same skeleton sequence usually possess strong inherent correlations. For example, they could locally share similar skeletons and partial sequences with consistent walking patterns. To exploit such intra-sequence relationships and inherent consistency (*e.g.*, pattern invariance) within sequences to learn better skeleton representations, we propose the **masked intra-sequence contrastive learning (MIC)** below.

Given two skeleton instances (*i.e.*, subsequence representations), $\mathbf{v}_{(i)}$ and $\mathbf{v}_{(j)}$, of the same sequence, we first map them into a contrasting space \mathbb{R}^H with a fully-connected (FC) layer $\mathcal{F}_c(\cdot)$ by: $\mathcal{F}_c(\mathbf{v}_{(i)}) = \mathbf{z}_{(i)}$ and $\mathcal{F}_c(\mathbf{v}_{(j)}) = \mathbf{z}_{(j)}$, where $\mathbf{z}_{(i)}, \mathbf{z}_{(j)} \in \mathbb{R}^H$. Inspired by [Chen and He, 2021], we leverage a Siamese architecture to contrast one instance in the original feature space with the other one in the new contrasting space, so as to *symmetrically* learn their inherent similarity. To this end, we exploit a masked intra-sequence contrastive learning (MIC) loss to minimize the negative cosine similarity between two instances of the same sequence by:

$$\mathcal{L}_{\text{MIC}} = -\alpha \frac{\mathbf{z}_{(i)} \cdot \mathbf{v}_{(j)}}{\|\mathbf{z}_{(i)}\|_2 \cdot \|\mathbf{v}_{(j)}\|_2} - \beta \frac{\mathbf{z}_{(j)} \cdot \mathbf{v}_{(i)}}{\|\mathbf{z}_{(j)}\|_2 \cdot \|\mathbf{v}_{(i)}\|_2}, \quad (6)$$

where $\|\cdot\|_2$ denotes ℓ_2 -norm, α and β are weights for contrastive learning of representation pairs $(\mathbf{z}_{(i)}, \mathbf{v}_{(j)})$ and $(\mathbf{z}_{(j)}, \mathbf{v}_{(i)})$, respectively. Here \mathcal{L}_{MIC} is defined for two subsequence representations of a skeleton sequence and the total loss is averaged over all sequences. To enable more stable and better contrastive learning, we employ a symmetrized loss with equal weights for two contrastive representation pairs,

i.e., $\alpha = \beta = 0.5$, and adopt an alternating stop-gradient operation following [Chen and He, 2021] when contrasting each pair, as shown in Fig. 2 (Note that we only visualize one contrastive pair for conciseness). We provide hypotheses and proof for the effectiveness of MIC in Appendix A.

3.3 The Entire Framework

The proposed SimMC framework combines both MPC loss (see Eq. (5)) and MIC loss (see Eq. (6)) to perform unsupervised contrastive learning of skeleton representations with:

$$\mathcal{L} = \lambda \mathcal{L}_{\text{MIC}} + (1 - \lambda) \mathcal{L}_{\text{MPC}}, \quad (7)$$

where λ is the weight coefficient to trade off the importance of different contrastive learning. For convenience, here we use \mathcal{L}_{MIC} to denote the total MIC loss averaging over all training skeleton sequences. To facilitate training and generate more reliable clusters, we optimize our model by alternating clustering and contrastive representation learning. For the person re-ID task, we exploit the encoder $\psi(\cdot)$ learned by our framework to encode each skeleton sequence of the probe set $\Phi_{\mathcal{P}}$ into corresponding representations, $\{\mathbf{v}_i^{\mathcal{P}}\}_{i=1}^{N_2}$, which are matched with the representations, $\{\mathbf{v}_j^{\mathcal{G}}\}_{j=1}^{N_3}$, of the same identity in the gallery set $\Phi_{\mathcal{G}}$ based on the Euclidean distance.

4 Experiments

4.1 Experimental Settings

Datasets: We evaluate our framework on four person re-ID benchmark datasets with 3D skeleton data, namely *IAS-Lab* [Munaro *et al.*, 2014b], *KS20* [Nambiar *et al.*, 2017], *BIWI* [Munaro *et al.*, 2014a], *KGBD* [Andersson and Araujo, 2015], and a large-scale multi-view gait dataset *CASIA-B* [Yu *et al.*, 2006], which contain 11, 20, 50, 164, and 124 different individuals, respectively. For BIWI and IAS-Lab, we set each testing set as the gallery and the other one as the probe. For KS20, we randomly take one skeleton sequence from each view as the probe sequence and use one half of the remaining sequences for training and the other half as the gallery. For KGBD, we randomly choose one skeleton video of each individual as the probe set, and equally divide the remaining videos into the training set and gallery set. In CASIA-B, all testing sequences are grouped by three conditions (Normal, Bags, Clothes), and we evaluate our framework with single-condition and cross-condition settings following [Liu *et al.*, 2015]. We repeat experiments with each setup for multiple times and report the average performance.

Implementation Details: We set sequence length f to 6 on IAS-Lab, KS20, BIWI, and KGBD datasets for a fair comparison with existing methods, and empirically employ $x = 2$ random masks for subsequence sampling. For the largest dataset CASIA-B with roughly estimated skeleton data from RGB videos, we set $f = 40$ with $x = 10$ random masks. The number of random subsequence sampling is $q = 2$ and the embedding size for skeleton representations is $H = 256$ for all datasets. We empirically set the temperature $\tau = 0.06$ (KGBD), $\tau = 0.07$ (BIWI), $\tau = 0.075$ (CASIA-B), $\tau = 0.08$ (KS20, IAS-Lab) for MPC learning, and adopt the weight coefficient $\lambda = 0.5$ for KS20, KGBD, and IAS-B, $\lambda = 0.75$

Table 1: Performance comparison with existing state-of-the-art skeleton-based methods on KS20, KGBD, and IAS-A. The amount of network parameters (million (M)) and computational complexity (giga floating-point operations (GFLOPs)) for the deep learning based methods are reported. “+ DF” denotes direct supervised fine-tuning. **Bold** refers to the best cases among self-supervised/unsupervised methods, while *italics* indicate achieving higher performance when exploiting SimMC (“+ SimMC”) to fine-tune corresponding pre-trained representations.

Types	Methods	# Params	GFLOPs	KS20				KGBD				IAS-A			
				top-1	top-5	top-10	mAP	top-1	top-5	top-10	mAP	top-1	top-5	top-10	mAP
Hand-crafted	D_{13} [Munaro <i>et al.</i> , 2014a]	—	—	39.4	71.7	81.7	18.9	17.0	34.4	44.2	1.9	40.0	58.7	67.6	24.5
	D_{16} [Pala <i>et al.</i> , 2019]	—	—	51.7	77.1	86.9	24.0	31.2	50.9	59.8	4.0	42.7	62.9	70.7	25.2
Supervised	PoseGait [Liao <i>et al.</i> , 2020]	8.93M	121.60	49.4	80.9	90.2	23.5	50.6	67.0	72.6	13.9	28.4	55.7	69.2	17.5
	SGELA [Rao <i>et al.</i> , 2021b] + DF	9.09M	7.48	49.7	67.0	77.1	22.2	43.7	58.7	65.0	7.1	18.0	32.1	46.2	13.5
	MG-SCR [Rao <i>et al.</i> , 2021d]	0.35M	6.60	46.3	75.4	84.0	10.4	44.0	58.7	64.6	6.9	36.4	59.6	69.5	14.1
	SM-SGE [Rao <i>et al.</i> , 2021a] + DF	6.25M	23.92	49.8	78.1	85.2	11.7	43.2	58.6	64.6	7.5	38.5	63.2	73.9	15.0
Self-supervised /Unsupervised	AGE [Rao <i>et al.</i> , 2020]	7.15M	37.37	43.2	70.1	80.0	8.9	2.9	5.6	7.5	0.9	31.1	54.8	67.4	13.4
	SGELA [Rao <i>et al.</i> , 2021b]	8.47M	7.47	45.0	65.0	75.1	21.2	37.2	53.5	60.0	4.5	16.7	30.2	44.0	13.2
	SM-SGE [Rao <i>et al.</i> , 2021a]	5.58M	22.61	45.9	71.9	81.2	9.5	31.4	50.6	58.4	4.4	27.4	57.0	69.8	13.3
	SimMC (Ours)	0.15M	0.99	66.4	80.7	87.0	22.3	54.9	66.2	70.6	11.7	44.8	65.3	72.9	18.7
Unsupervised Fine-tuning	SGELA + SimMC	8.80M	10.10	47.3	69.7	79.3	20.1	51.7	62.7	67.9	15.1	16.8	33.3	48.7	12.0
	MG-SCR + SimMC	0.53M	6.49	71.1	83.6	89.1	22.7	47.4	59.3	64.9	11.0	47.2	69.0	77.3	22.4
	SM-SGE + SimMC	5.89M	25.10	67.2	82.2	88.5	23.0	47.1	59.2	64.9	10.8	51.3	69.9	75.6	27.3

Table 2: Performance comparison on IAS-B, BIWI-Walking (BIWI-W), and BIWI-Still (BIWI-S). **Bold** refers to the best cases among self-supervised/unsupervised methods, while *italics* indicate achieving higher performance with the fine-tuning of SimMC.

Types	Methods	IAS-B				BIWI-W				BIWI-S			
		top-1	top-5	top-10	mAP	top-1	top-5	top-10	mAP	top-1	top-5	top-10	mAP
Hand-crafted	D_{13} [Munaro <i>et al.</i> , 2014a]	43.7	68.6	76.7	23.7	14.2	20.6	23.7	17.2	28.3	53.1	65.9	13.1
	D_{16} [Pala <i>et al.</i> , 2019]	44.5	69.1	80.2	24.5	17.0	25.3	29.6	18.8	32.6	55.7	68.3	16.7
Supervised	PoseGait [Liao <i>et al.</i> , 2020]	28.9	51.6	62.9	20.8	8.8	23.0	31.2	11.1	14.0	40.7	56.7	9.9
	SGELA [Rao <i>et al.</i> , 2021b] + DF	23.6	42.9	51.9	14.8	13.9	15.3	16.7	22.9	29.2	65.2	73.8	23.5
	MG-SCR [Rao <i>et al.</i> , 2021d]	32.4	56.5	69.4	12.9	10.8	20.3	29.4	11.9	20.1	46.9	64.1	7.6
	SM-SGE [Rao <i>et al.</i> , 2021a] + DF	44.3	68.2	77.5	14.9	16.7	31.0	40.2	18.7	34.8	60.6	71.5	12.8
Self-supervised /Unsupervised	AGE [Rao <i>et al.</i> , 2020]	31.1	52.3	64.2	12.8	11.7	21.4	27.3	12.6	25.1	43.1	61.6	8.9
	SGELA [Rao <i>et al.</i> , 2021b]	22.2	40.8	50.2	14.0	11.7	14.0	14.7	19.0	25.8	51.8	64.4	15.1
	SM-SGE [Rao <i>et al.</i> , 2021a]	38.9	64.1	75.8	13.3	13.2	25.8	33.5	15.2	31.3	56.3	69.1	10.1
	SimMC (Ours)	46.3	68.1	77.0	22.9	24.5	36.7	44.5	19.9	41.7	66.6	76.8	12.3
Unsupervised Fine-tuning	SGELA + SimMC	21.2	39.1	48.8	14.0	18.4	23.1	25.0	28.7	51.8	71.3	74.4	43.3
	MG-SCR + SimMC	52.4	72.0	78.8	29.1	25.1	37.5	46.4	20.3	28.3	51.6	64.8	10.9
	SM-SGE + SimMC	55.3	72.6	80.3	34.1	25.9	39.2	45.2	22.4	42.6	64.8	76.2	15.4

for IAS-A, and $\lambda = 0.25$ for BIWI and CASIA-B. We employ Adam optimizer with learning rate 0.00035 and batch size 256 for all datasets. To perform unsupervised fine-tuning with SimMC, we train SimMC on the unlabeled skeleton representations pre-trained by original models, and exploit the skeleton representations learned by SimMC for person re-ID. More implementation details are provided in Appendix B.

Evaluation Metrics: We compute Cumulative Matching Characteristics (CMC) curve and adopt top-1/top-5/top-10 accuracy and Mean Average Precision (mAP) [Zheng *et al.*, 2015] to quantitatively evaluate person re-ID performance.

4.2 Comparison with State-of-the-Arts

We compare our framework with existing state-of-the-art self-supervised and unsupervised skeleton-based methods on KS20, KGBD, IAS-Lab, and BIWI in Table 1 and 2. We also include the latest supervised skeleton-based methods and representative hand-crafted methods as a performance reference.

Comparison with Self-supervised and Unsupervised Methods: Our framework shows evident advantages in terms of performance and efficiency over existing state-of-the-art self-supervised and unsupervised methods. As reported in Table 1 and 2, SimMC significantly outperforms AGE [Rao *et al.*, 2020] and SM-SGE [Rao *et al.*, 2021a] that manually design pretext tasks based on pre-defined skeleton modeling such as skeleton graphs by a large margin of 7.4-52.0% top-1 accuracy and 2.2-13.4% mAP on all datasets. Compared with the SGELA model [Rao *et al.*, 2021b] using direct inter-sequence contrastive learning, our framework achieves

remarkably better performance on five out of six testing sets (KS20, KGBD, IAS-A, IAS-B, BIWI-W) by up to 28.1% top-1 accuracy and 8.9% mAP, which demonstrates that the proposed SimMC combining both prototype (MPC) and intra-sequence contrastive learning (MIC) can capture more discriminative features within skeleton sequences for person re-ID on different datasets. Notably, SimMC also enjoys the smallest model size (only 0.15M) for skeleton representation learning among all approaches shown in Table 1, which suggests its higher model efficiency for person re-ID tasks.

By applying the proposed framework to fine-tuning SGELA and SM-SGE models, we can further improve their performance with an average gain of 16.9% and 8.1% top-1 accuracy respectively on all datasets. Such results demonstrate both effectiveness and scalability of proposed masked contrastive learning, which is compatible with existing models and can fully exploit their pre-trained features to achieve higher-quality skeleton representations for person re-ID.

Comparison with Hand-crafted and Supervised Methods: In contrast to hand-crafted methods (D_{13} and D_{16}) that rely on geometric joint distances and anthropometric descriptors, our approach obtains similar performance on IAS testing sets, while it achieves a distinct improvement of 7.5-37.9% top-1 accuracy on BIWI, KS20, and KGBD datasets that contain more views and individuals. Despite utilizing *unlabeled* skeleton data as the sole input, the proposed SimMC still performs better than the latest supervised models PoseGait and MG-SCR in most cases. Interestingly, applying SimMC to SM-SGE achieves significantly higher performance gains

Table 3: Comparison with appearance-based and skeleton-based methods on CASIA-B. “Bags-Normal” represents the probe set with “Bags” condition and gallery set with “Normal” condition. “—” indicates no published result. Full results are in Appendix B.

Probe-Gallery	Normal-Normal				Bags-Bags				Clothes-Clothes				Clothes-Normal				Bags-Normal			
Methods	top-1	top-5	top-10	mAP	top-1	top-5	top-10	mAP	top-1	top-5	top-10	mAP	top-1	top-5	top-10	mAP	top-1	top-5	top-10	mAP
ELF [Gray and Tao, 2008]	12.3	35.6	50.3	—	5.8	25.5	37.6	—	19.9	43.9	56.7	—	5.6	16.0	26.3	—	17.1	30.0	37.9	—
SDALF [Farenzena <i>et al.</i> , 2010]	4.9	27.0	41.6	—	10.2	33.5	47.2	—	16.7	42.0	56.7	—	11.6	19.4	27.6	—	22.9	30.1	36.1	—
MLR [Liu <i>et al.</i> , 2015]	16.3	43.4	60.8	—	18.9	44.8	59.4	—	25.4	53.3	68.9	—	20.3	42.6	56.9	—	31.8	53.6	64.1	—
AGE [Rao <i>et al.</i> , 2020]	20.8	29.3	34.2	3.5	37.1	56.2	67.0	9.8	35.5	54.3	65.3	9.6	14.6	33.0	42.7	3.0	32.4	51.2	60.1	3.9
SM-SGE [Rao <i>et al.</i> , 2021a]	50.2	73.5	81.9	6.6	26.6	49.0	59.4	9.3	27.2	51.4	63.2	9.7	10.6	26.3	35.9	3.0	16.6	36.8	47.5	3.5
SGELA [Rao <i>et al.</i> , 2021b]	71.8	87.5	91.4	9.8	48.1	69.5	77.7	16.5	51.2	73.8	81.5	7.1	15.9	30.8	40.6	4.7	36.4	57.1	64.6	6.7
SimMC (Ours)	84.8	92.3	93.7	10.8	69.1	86.6	91.3	16.5	68.0	88.1	93.0	15.7	25.6	43.8	54.0	5.4	42.0	59.8	68.9	7.1

Table 4: Ablation study of framework with different configurations: Naïve prototype contrastive learning (NPC) using only original sequences, masked prototype contrastive learning (MPC) scheme and corresponding masked intra-sequence contrastive learning (MIC).

Configurations	IAS-A		IAS-B		BIWI-S		BIWI-W		KS20		KGBD	
	top-1	mAP	top-1	mAP	top-1	mAP	top-1	mAP	top-1	mAP	top-1	mAP
Baseline	29.4	13.8	30.2	13.3	24.8	9.3	10.9	14.1	17.0	9.5	34.5	6.4
NPC	39.2	17.8	40.7	21.5	38.1	11.3	21.2	18.3	64.8	20.5	53.0	11.0
MPC	43.1	18.5	43.8	22.3	40.1	11.7	23.7	19.5	65.6	21.1	53.6	11.0
MPC + MIC	44.8	18.7	46.3	22.9	41.7	12.3	24.5	19.9	66.4	22.3	54.9	11.7

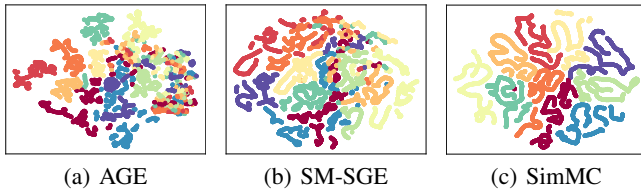


Figure 3: t-SNE visualization of representations learned by AGE (a), SM-SGE (b), and SimMC (c) for first ten classes in BIWI. Different colors denote skeleton representations of different classes.

than direct supervised fine-tuning (DF) in terms of top-1 accuracy (3.9-17.4%), top-5 accuracy (0.6-6.7%), top-10 accuracy (0.3-5.0%), and mAP (3.3-19.2%) on all datasets. With highly efficient performance and strong scalability, the proposed unsupervised SimMC can be a more general framework for skeleton-based person re-ID and related tasks.

5 Further Analysis

Application to Model-estimated Skeletons. To verify the effectiveness of SimMC when applied to RGB-based scenes with model-estimated 3D skeletons, we utilize pre-trained pose estimation models to extract skeleton data from RGB videos of CASIA-B, and compare the performance of SimMC with representative appearance-based and skeleton-based methods. As shown in Table 3, the proposed SimMC remarkably outperforms state-of-the-art skeleton-based models SM-SGE and SGELA by a distinct margin of 5.6% to 42.5% top-1 accuracy and 0.4% to 8.6% mAP in different conditions, which suggests the stronger ability of our framework on capturing discriminative features from estimated skeleton data for person re-ID. Compared with appearance-based ELF and MLR models that utilize visual features (*e.g.*, colors, textures, and silhouettes) with extra label information, the skeleton-based SimMC also achieves superior performance in all conditions of CASIA-B, which demonstrates its great applicable value and potential for person re-ID under large-scale RGB-based scenarios and more general settings.

Ablation Study. We conduct ablation study to demon-

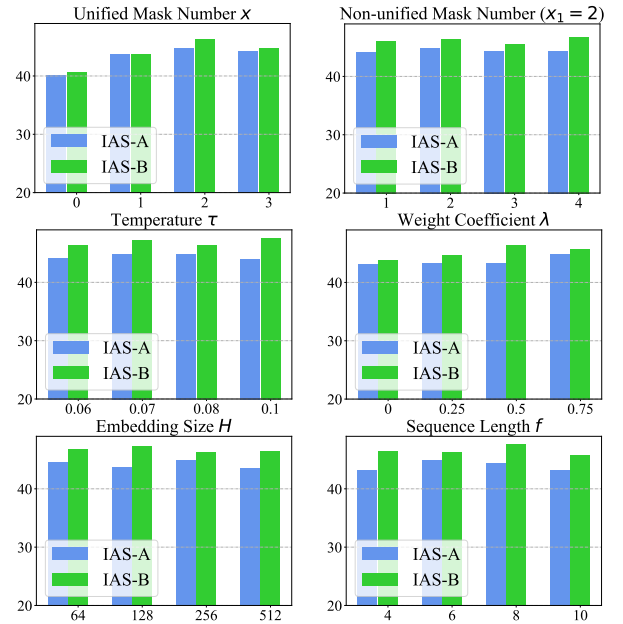


Figure 4: Top-1 accuracy on IAS-A/B showing effects of hyperparameters. “Non-unified Mask Number ($x_1 = 2$)” denotes using different mask numbers including $x = 2$ for subsequence sampling.

strate the contribution of each component in our framework. We adopt 3D coordinates of raw skeleton sequences as the baseline representation for person re-ID. As reported in Table 4, the model exploiting NPC significantly outperforms the baseline by 9.8-47.8% top-1 accuracy and 2.0-11.0% mAP. Considering that NPC is a special case of the proposed MPC scheme (see Sec. 3.1), such results verify the effectiveness of the skeleton prototype contrastive learning in MPC, which can capture highly discriminative features within unlabeled skeleton sequences for the task of person re-ID. Employing the standard MPC scheme with randomly sampled subsequences consistently improves the model performance by up to 3.9% top-1 accuracy and 1.2% mAP on all datasets, which demonstrates that MPC is able to mine more representative

key features from skeleton subsequences to perform person re-ID. Finally, incorporating MIC into MPC further improves model performance with 0.8-2.5% top-1 accuracy and 0.2%-1.2% mAP gains on different datasets. This justifies our claim that capturing inherent intra-sequence similarity and pattern consistency within sequences could facilitate learning better representations of skeleton sequences for person re-ID.

Discussions. As shown in Fig. 3, we conduct a t-SNE visualization [Van der Maaten and Hinton, 2008] of representations. The skeleton representations learned by our framework are clustered with higher inter-class separation than AGE and SM-SGE, which suggests that SimMC may learn richer class-related semantics and lower-entropy skeleton representations. We also show effects of different parameters on SimMC in Fig. 4, which indicates that the use of random masks ($x > 0$) is the key to the proposed masked contrastive learning, regardless of adopting unified or non-unified mask numbers, while an appropriate fusion ($\lambda > 0$) of MIC and MPC facilitates better skeleton representation learning for person re-ID. Our framework with the optimal parameter setting is not sensitive to changes of some parameters such as temperatures τ . More results and proof are provided in the appendices.

6 Conclusion

In this paper, we propose a simple masked contrastive learning (SimMC) framework to efficiently learn representations of unlabeled skeleton sequences for unsupervised person re-ID. A novel masked prototype contrastive learning (MPC) scheme is devised to cluster the most typical skeleton features of subsequences randomly masked from original sequences, so as to contrast their inherent similarity to learn a discriminative skeleton representation from unlabeled skeletons. To fully exploit inherent relationships between subsequences, we propose a masked intra-sequence contrastive learning (MIC) to learn their similarity and pattern consistency within the sequence for more effective skeleton representations. Our framework outperforms existing state-of-the-art skeleton-based methods and also enjoys high scalability and efficiency to be applied to different models and scenes.

7 Ethics Statement

Person re-ID as an important emerging research topic possesses great value for both academia and industry. However, illegal or improper use of person re-ID technologies could pose serious threat to the public privacy and society security. Therefore, it should be noted that all datasets used in our experiments are officially shared by reliable public (IAS-Lab, BIWI, KGBD) or private research agency (KS20, CASIA-B), which have guaranteed that the collecting, processing, releasing, and using of all data are with the consent of participated subjects. For the protection of privacy, all individuals are anonymized with simple identity numbers. Our models and codes must only be used for the purpose of research.

Acknowledgements

This work was supported by Alibaba Group through Alibaba Innovative Research (AIR) Program and Alibaba-NTU Sin-

gapore Joint Research Institute (JRI), Nanyang Technological University, Singapore.

References

- [Andersson and Araujo, 2015] Virginia Ortiz Andersson and Ricardo Matsumura Araujo. Person identification using anthropometric and gait data from kinect sensor. In *AAAI*, 2015.
- [Barbosa *et al.*, 2012] Igor Barros Barbosa, Marco Cristani, Alessio Del Bue, Loris Bazzani, and Vittorio Murino. Re-identification with rgb-d sensors. In *ECCV*, pages 433–442. Springer, 2012.
- [Chen and He, 2021] Xinlei Chen and Kaiming He. Exploring simple siamese representation learning. In *CVPR*, pages 15750–15758, 2021.
- [Chen *et al.*, 2020] Ting Chen, Simon Kornblith, Mohammad Norouzi, and Geoffrey Hinton. A simple framework for contrastive learning of visual representations. In *ICML*, 2020.
- [Ester *et al.*, 1996] Martin Ester, Hans-Peter Kriegel, Jörg Sander, Xiaowei Xu, et al. A density-based algorithm for discovering clusters in large spatial databases with noise. In *KDD*, volume 96, pages 226–231, 1996.
- [Farenzena *et al.*, 2010] Michela Farenzena, Loris Bazzani, Alessandro Perina, Vittorio Murino, and Marco Cristani. Person re-identification by symmetry-driven accumulation of local features. In *CVPR*, pages 2360–2367. IEEE, 2010.
- [Gray and Tao, 2008] Douglas Gray and Hai Tao. Viewpoint invariant pedestrian recognition with an ensemble of localized features. In *ECCV*, pages 262–275. Springer, 2008.
- [Han *et al.*, 2017] Fei Han, Brian Reily, William Hoff, and Hao Zhang. Space-time representation of people based on 3d skeletal data: A review. *Computer Vision and Image Understanding*, 158:85–105, 2017.
- [He *et al.*, 2020] Kaiming He, Haoqi Fan, Yuxin Wu, Saining Xie, and Ross Girshick. Momentum contrast for unsupervised visual representation learning. In *CVPR*, pages 9729–9738, 2020.
- [Li *et al.*, 2021] Junnan Li, Pan Zhou, Caiming Xiong, and Steven Hoi. Prototypical contrastive learning of unsupervised representations. In *ICLR*, 2021.
- [Liao *et al.*, 2020] Rijun Liao, Shiqi Yu, Weizhi An, and Yongzhen Huang. A model-based gait recognition method with body pose and human prior knowledge. *Pattern Recognition*, 98:107069, 2020.
- [Liu *et al.*, 2015] Zheng Liu, Zhaoxiang Zhang, Qiang Wu, and Yunhong Wang. Enhancing person re-identification by integrating gait biometric. *Neurocomputing*, 168:1144–1156, 2015.
- [Munaro *et al.*, 2014a] Matteo Munaro, Andrea Fossati, Alberto Basso, Emanuele Menegatti, and Luc Van Gool. One-shot person re-identification with a consumer depth camera. In *Person Re-Identification*, pages 161–181. Springer, 2014.

- [Munaro *et al.*, 2014b] Matteo Munaro, Stefano Ghidoni, Deniz Tartaro Dizmen, and Emanuele Menegatti. A feature-based approach to people re-identification using skeleton keypoints. In *ICRA*, pages 5644–5651. IEEE, 2014.
- [Murray *et al.*, 1964] M Pat Murray, A Bernard Drought, and Ross C Kory. Walking patterns of normal men. *Journal of Bone and Joint Surgery*, 46(2):335–360, 1964.
- [Nambiar *et al.*, 2017] Athira Nambiar, Alexandre Bernardino, Jacinto C Nascimento, and Ana Fred. Context-aware person re-identification in the wild via fusion of gait and anthropometric features. In *International Conference on Automatic Face & Gesture Recognition*, pages 973–980. IEEE, 2017.
- [Oord *et al.*, 2018] Aaron van den Oord, Yazhe Li, and Oriol Vinyals. Representation learning with contrastive predictive coding. *arXiv preprint arXiv:1807.03748*, 2018.
- [Pala *et al.*, 2019] Pietro Pala, Lorenzo Seidenari, Stefano Berretti, and Alberto Del Bimbo. Enhanced skeleton and face 3d data for person re-identification from depth cameras. *Computers & Graphics*, 2019.
- [Rao *et al.*, 2020] Haocong Rao, Siqu Wang, Xiping Hu, Mingkui Tan, Huang Da, Jun Cheng, and Bin Hu. Self-supervised gait encoding with locality-aware attention for person re-identification. In *IJCAI*, volume 1, pages 898–905, 2020.
- [Rao *et al.*, 2021a] Haocong Rao, Xiping Hu, Jun Cheng, and Bin Hu. Sm-sge: A self-supervised multi-scale skeleton graph encoding framework for person re-identification. In *Proceedings of the 29th ACM international conference on Multimedia*, 2021.
- [Rao *et al.*, 2021b] Haocong Rao, Siqu Wang, Xiping Hu, Mingkui Tan, Yi Guo, Jun Cheng, Xinwang Liu, and Bin Hu. A self-supervised gait encoding approach with locality-awareness for 3d skeleton based person re-identification. *IEEE Transactions on Pattern Analysis and Machine Intelligence*, 2021.
- [Rao *et al.*, 2021c] Haocong Rao, Shihao Xu, Xiping Hu, Jun Cheng, and Bin Hu. Augmented skeleton based contrastive action learning with momentum lstm for unsupervised action recognition. *Information Sciences*, 569:90–109, 2021.
- [Rao *et al.*, 2021d] Haocong Rao, Shihao Xu, Xiping Hu, Jun Cheng, and Bin Hu. Multi-level graph encoding with structural-collaborative relation learning for skeleton-based person re-identification. In *IJCAI*, 2021.
- [Van der Maaten and Hinton, 2008] Laurens Van der Maaten and Geoffrey Hinton. Visualizing data using t-sne. *Journal of machine learning research*, 9(11), 2008.
- [Wu *et al.*, 2018] Zhirong Wu, Yuanjun Xiong, Stella X Yu, and Dahua Lin. Unsupervised feature learning via non-parametric instance discrimination. In *CVPR*, pages 3733–3742, 2018.
- [Ye *et al.*, 2021] Mang Ye, Jianbing Shen, Gaojie Lin, Tao Xiang, Ling Shao, and Steven CH Hoi. Deep learning for person re-identification: A survey and outlook. *IEEE Transactions on Pattern Analysis and Machine Intelligence*, 2021.
- [Yu *et al.*, 2006] Shiqi Yu, Daoliang Tan, and Tieniu Tan. A framework for evaluating the effect of view angle, clothing and carrying condition on gait recognition. In *ICPR*, volume 4, pages 441–444. IEEE, 2006.
- [Zheng *et al.*, 2015] Liang Zheng, Liye Shen, Lu Tian, Shengjin Wang, Jingdong Wang, and Qi Tian. Scalable person re-identification: A benchmark. In *ICCV*, pages 1116–1124, 2015.

SimMC: Simple Masked Contrastive Learning of Skeleton Representations for Unsupervised Person Re-Identification - Appendix A Proof

Haocong Rao and Chunyan Miao[†]

School of Computer Science and Engineering, Nanyang Technological University
Joint NTU-UBC Research Centre of Excellence in Active Living for the Elderly (LILY)
haocong001@ntu.edu.sg, ascymiao@ntu.edu.sg

The proposed masked prototype contrastive learning (MPC) and masked intra-sequence contrastive learning (MIC) can be formulated as Expectation-Maximization (EM) solutions. In this Appendix, we provide a theoretical EM modeling for each component of the proposed framework to prove its effectiveness and convergence.

I Masked Prototype Contrastive Learning (MPC) as Expectation-Maximization

Preliminary. For clarity and convenience, we adopt a more general set of notations here, which are different from those used in the paper. Suppose that a training set $X = \{\mathbf{x}_i\}_{i=1}^N$ contains N skeleton sequences, where $\mathbf{x}_i \in \mathbb{R}^{f \times K}$, the objective of unsupervised skeleton representation learning is to learn an embedding/encoder function f_θ (realized via θ -parameterized neural networks) that maps X to $V = \{\mathbf{v}_i\}_{i=1}^N$, where $\mathbf{v}_i \in \mathbb{R}^H$, by $\mathbf{v}_i = f_\theta(\mathbf{x}_i)$ without using any label, such that \mathbf{v}_i can effectively represent features of \mathbf{x}_i to perform person re-identification.

Formally, the goal is to find the network parameters θ that maximizes the log-likelihood function of the observed N skeleton sequences as follows:

$$\begin{aligned} \theta^* &= \arg \max_{\theta} L(\mathbf{x}_1, \dots, \mathbf{x}_N; \theta) \\ &= \arg \max_{\theta} \prod_{i=1}^N p(\mathbf{x}_i; \theta) \iff \arg \max_{\theta} \sum_{i=1}^N \log p(\mathbf{x}_i; \theta), \end{aligned} \quad (1)$$

where $L(\mathbf{x}_1, \dots, \mathbf{x}_N; \theta)$ denotes the likelihood function of the observed skeleton sequences $\{\mathbf{x}_i\}_{i=1}^N$ w.r.t θ , and each skeleton sequence \mathbf{x}_i is hypothetically related to a certain skeleton prototype $\mathbf{c}_j \in \mathbb{R}^H$ and $\mathbf{c}_j \in \{\mathbf{c}_j\}_{j=1}^K$. Under this assumption, we can re-formulate the objective in Eq. (1) as:

$$\begin{aligned} \theta^* &= \arg \max_{\theta} \sum_{i=1}^N \log p(\mathbf{x}_i; \theta) \\ &= \arg \max_{\theta} \sum_{i=1}^N \log \sum_{j=1}^K p(\mathbf{x}_i, \mathbf{c}_j; \theta), \end{aligned} \quad (2)$$

Directly optimizing this function is intractable, thus we take its lower-bound by using a surrogate function as:

$$\begin{aligned} \sum_{i=1}^N \log \sum_{j=1}^K p(\mathbf{x}_i, \mathbf{c}_j; \theta) &= \sum_{i=1}^N \log \sum_{j=1}^K Q(\mathbf{c}_j) \frac{p(\mathbf{x}_i, \mathbf{c}_j; \theta)}{Q(\mathbf{c}_j)} \\ &\geq \sum_{i=1}^N \sum_{j=1}^K Q(\mathbf{c}_j) \log \frac{p(\mathbf{x}_i, \mathbf{c}_j; \theta)}{Q(\mathbf{c}_j)}, \end{aligned} \quad (3)$$

where $Q(\mathbf{c}_j)$ represents some distribution over $\{\mathbf{c}_j\}_{j=1}^K$ and $\sum_{j=1}^K Q(\mathbf{c}_j) = 1$. We apply Jensen's inequality to deriving the last step, where the equality can be achieved under the condition that $\frac{p(\mathbf{x}_i, \mathbf{c}_j; \theta)}{Q(\mathbf{c}_j)}$ is a constant. To realize this equality, we have:

$$Q(\mathbf{c}_j) = \frac{p(\mathbf{x}_i, \mathbf{c}_j; \theta)}{\sum_{j=1}^K p(\mathbf{x}_i, \mathbf{c}_j; \theta)} = \frac{p(\mathbf{x}_i, \mathbf{c}_j; \theta)}{p(\mathbf{x}_i; \theta)} = p(\mathbf{c}_j; \mathbf{x}_i, \theta), \quad (4)$$

where $Q(\mathbf{c}_j)$ is a posterior probability related to $\mathbf{c}_j, \mathbf{x}_i$, and θ . When θ is fixed at the Expectation step, the distribution of representations (\mathbf{x}_i) and corresponding prototypes (\mathbf{c}_j) can be estimated as a result of clustering, thus we can get the constant value of $Q(\mathbf{c}_j) = p(\mathbf{c}_j; \mathbf{x}_i, \theta)$ based on the result. We can re-write Eq. (3) as:

$$\sum_{i=1}^N \sum_{j=1}^K (Q(\mathbf{c}_j) \log p(\mathbf{x}_i, \mathbf{c}_j; \theta) - Q(\mathbf{c}_j) \log Q(\mathbf{c}_j)), \quad (5)$$

where the constant $-\sum_{i=1}^N \sum_{j=1}^K Q(\mathbf{c}_j) \log Q(\mathbf{c}_j)$ can be ignored and we need to maximize:

$$\sum_{i=1}^N \sum_{j=1}^K Q(\mathbf{c}_j) \log p(\mathbf{x}_i, \mathbf{c}_j; \theta) \quad (6)$$

For Expectation (E)-step, we aim to estimate $p(\mathbf{c}_j; \mathbf{x}_i, \theta)$ (see Eq. (4)). In our framework, we perform DBSCAN algorithm on the features $\mathbf{v}_i = f_\theta(\mathbf{x}_i)$ given by the encoder to obtain K clusters $\{\mathbf{C}_j\}_{j=1}^K$. We generate corresponding skeleton prototype \mathbf{c}_j , which is the centroid of the j^{th} cluster \mathbf{C}_j . Then, we compute $p(\mathbf{c}_j; \mathbf{x}_i, \theta) = \mathbb{1}(\mathbf{x}_i \in \mathbf{C}_j)$,

[†]Corresponding author

where $\mathbb{1}(\mathbf{x}_i \in \mathbf{C}_j) = 1$ if \mathbf{x}_i belongs to the j^{th} cluster \mathbf{C}_j (*i.e.*, corresponding to skeleton prototype \mathbf{c}_j); otherwise $\mathbb{1}(\mathbf{x}_i \in \mathbf{C}_j) = 0$.

In **Maximization (M)-step**, we combine Eq. (4) to maximize the lower-bound in Eq. (6) after the E-step:

$$\begin{aligned} & \sum_{i=1}^N \sum_{j=1}^K Q(\mathbf{c}_j) \log p(\mathbf{x}_i, \mathbf{c}_j; \theta) \\ &= \sum_{i=1}^N \sum_{j=1}^K p(\mathbf{c}_j; \mathbf{x}_i, \theta) \log p(\mathbf{x}_i, \mathbf{c}_j; \theta) \\ &= \sum_{i=1}^N \sum_{j=1}^K \mathbb{1}(\mathbf{x}_i \in \mathbf{C}_j) \log p(\mathbf{x}_i, \mathbf{c}_j; \theta) \end{aligned} \quad (7)$$

Each cluster centroid \mathbf{c}_j is assumed with a uniform prior probability $p(\mathbf{c}_j; \theta) = \frac{1}{k}$ since we are not provided any samples. We have:

$$p(\mathbf{x}_i, \mathbf{c}_j; \theta) = p(\mathbf{x}_i; \mathbf{c}_j, \theta) p(\mathbf{c}_j; \theta) = \frac{1}{k} \cdot p(\mathbf{x}_i; \mathbf{c}_j, \theta), \quad (8)$$

where the distribution of samples around each prototype is assumed as an isotropic Gaussian, leading to:

$$p(\mathbf{x}_i; \mathbf{c}_j, \theta) = \frac{\exp\left(-\frac{(\mathbf{v}_i - \mathbf{c}_p)^2}{2\sigma_p^2}\right)}{\sum_{j=1}^K \exp\left(-\frac{(\mathbf{v}_i - \mathbf{c}_j)^2}{2\sigma_j^2}\right)}, \quad (9)$$

where $\mathbf{v}_i = f_\theta(\mathbf{x}_i)$ and \mathbf{c}_p is the prototype for the cluster \mathbf{C}_p containing \mathbf{x}_i , *i.e.*, $\mathbf{x}_i \in \mathbf{C}_p$. We apply ℓ_2 -normalization to both \mathbf{v} and \mathbf{c} to have $(\mathbf{v} - \mathbf{c})^2 = 2 - 2\mathbf{v} \cdot \mathbf{c}$. Then combining this with Eq. (2), (3), (6), (7), (8), and (9), we can get the maximum log-likelihood estimation with:

$$\begin{aligned} \theta^* &= \arg \min_{\theta} \sum_{i=1}^N -\log \frac{\exp(\mathbf{v}_i \cdot \mathbf{c}_p / \tau_p)}{\sum_{j=1}^K \exp(\mathbf{v}_i \cdot \mathbf{c}_j / \tau_j)} \\ \Leftrightarrow \theta^* &= \arg \min_{\theta} \sum_{k=1}^K \sum_{i=1}^{N_k} -\log \frac{\exp(\mathbf{v}_i^k \cdot \mathbf{c}_k / \tau_k)}{\sum_{j=1}^K \exp(\mathbf{v}_i^k \cdot \mathbf{c}_j / \tau_j)}, \end{aligned} \quad (10)$$

where \mathbf{v}_i^k denotes the representation of i^{th} sample (*i.e.*, skeleton sequence) belonging to the k^{th} prototype \mathbf{c}_k , N_k is the number of samples in the k^{th} cluster, and τ is related to the distribution of features around different prototypes.

Relations to Existing Contrastive Losses: (1) The InfoNCE loss [Oord *et al.*, 2018] used or re-formulated in MoCo [He *et al.*, 2020] and SimCLR [Chen *et al.*, 2020] can be interpreted as special cases of the maximum log-likelihood estimation in Eq. (10), where the prototype \mathbf{c}_p for a feature \mathbf{v}_i is replaced by the augmented feature \mathbf{v}'_i generated from different views of augmentation of the same instance (*i.e.*, $\mathbf{c}_p = \mathbf{v}'_i$) and τ is fixed as a temperature for contrastive learning. (2) The ProtoNCE loss used in PCL [Li *et al.*, 2021] has a similar form as Eq. (10), where τ is estimated with the assumption that the distribution of feature representations around each prototype varies in different clusters. However,

such estimation could be inapplicable when employing different clustering algorithms* (*e.g.*, density-based DBSCAN [Ester *et al.*, 1996]) and results in unsatisfactory performance in practice.

In our work, we adopt a generic form following InfoNCE loss, *i.e.*, setting a global temperature τ , for the proposed SimMC framework. By assuming a uniform feature distribution around each instance (*i.e.*, $\tau = \tau_k = \tau_j$), we select an appropriate τ to encourage the framework to learn representations with higher global uniformity, which could improve the quality of contrastive representation learning as proved in [Wang and Isola, 2020; Gao *et al.*, 2021]. We show the effective of our framework on enhancing the uniformity of skeleton representation space in the Appendix B.

In the proposed framework, we sample q subsequences of length $(f - x)$ by applying x random masks to each input skeleton sequence. Specifically, we generate q sets of subsequences for the whole training set by randomly sampling one subsequence for each training sequence at each round of q sampling rounds, which are encoded into corresponding skeleton instance sets by the embedding/encoder function $f_\theta(\cdot)$. Then we independently perform clustering on each instance set to obtain corresponding skeleton prototypes. The random subsequence sampling and multiple individual clustering encourage a more stable probability estimation of skeleton prototypes and facilitate mining more valuable intra-sequence skeleton features and high-level semantics (*e.g.*, class-related semantics) within skeleton sequences. We can formulate the proposed masked prototype contrastive (MPC) loss based on Eq. (10) with:

$$\mathcal{L}_{\text{MPC}} = \frac{1}{N} \sum_{i=1}^q \sum_{k=1}^{K_i} \sum_{j=1}^{N_k} -\log \frac{\exp(\mathbf{v}_{(i),j}^k \cdot \mathbf{c}_{(i)}^k / \tau)}{\sum_{u=1}^{K_i} \exp(\mathbf{v}_{(i),j}^k \cdot \mathbf{c}_{(i)}^u / \tau)}, \quad (11)$$

where N represents the number of all training instances, K_i denotes the number of skeleton prototypes generated from the i^{th} set of subsequence representations, N_k is the number of skeleton instances belonging to the k^{th} prototype $\mathbf{c}_{(i)}^k$ (equivalent to $\mathbf{p}_{(i)}^k$ in the paper), and τ represents the global temperature for contrastive learning. When we utilize the original sequences without sampled subsequences for skeleton prototype learning, *i.e.*, $q = 1$ and $x = 0$ (see Eq. (2) and (3) in paper), the objective of Eq. (11) has exactly the same form as Eq. (10), which is defined as naïve prototype contrastive learning (denoted as NPC) in our paper. Therefore, the proposed MPC scheme could be viewed as to perform finer prototype contrastive learning with different subsequences (*i.e.*, NPC using original sequences is a special case of MPC), and allows the model to jointly attend to key skeleton patterns from different representation subspaces of the original sequences, which facilitates learning more discriminative skeleton representations for person re-ID, as demonstrated in our paper.

*PCL [Li *et al.*, 2021] adopts the distance-based k -means clustering and estimates the feature distribution using Euclidean distance.

I.1 Convergence Proof

We provide the proof for the convergence of the proposed MPC under the modeling of the maximum log-likelihood estimation (see Eq. (10)). Recall Eq. (2) and (3) and let

$$\begin{aligned}\ell(\theta) &= \sum_{i=1}^N \log p(\mathbf{x}_i; \theta) = \sum_{i=1}^N \log \sum_{j=1}^K p(\mathbf{x}_i, \mathbf{c}_j; \theta) \\ &= \sum_{i=1}^N \log \sum_{j=1}^K Q(\mathbf{c}_j) \frac{p(\mathbf{x}_i, \mathbf{c}_j; \theta)}{Q(\mathbf{c}_j)} \\ &\geq \sum_{i=1}^N \sum_{j=1}^K Q(\mathbf{c}_j) \log \frac{p(\mathbf{x}_i, \mathbf{c}_j; \theta)}{Q(\mathbf{c}_j)}\end{aligned}\quad (12)$$

The above inequality holds with equality when $Q(\mathbf{c}_j) = p(\mathbf{c}_j; \mathbf{x}_i, \theta)$ is a constant (see Eq. (4)).

In the t^{th} E-step, we have estimated the constant value $Q^{(t)}(\mathbf{c}_j) = p(\mathbf{c}_j; \mathbf{x}_i, \theta^{(t)})$. Then we have:

$$\ell(\theta^{(t)}) = \sum_{i=1}^N \sum_{j=1}^K Q^{(t)}(\mathbf{c}_j) \log \frac{p(\mathbf{x}_i, \mathbf{c}_j; \theta^{(t)})}{Q^{(t)}(\mathbf{c}_j)} \quad (13)$$

For the t^{th} M-step, we fix $Q^{(t)}(\mathbf{c}_j) = p(\mathbf{c}_j; \mathbf{x}_i, \theta^{(t)})$ and train model parameters θ to maximize Eq. (13). In this way, we can always have:

$$\begin{aligned}\ell(\theta^{(t+1)}) &\geq \sum_{i=1}^N \sum_{j=1}^K Q^{(t)}(\mathbf{c}_j) \log \frac{p(\mathbf{x}_i, \mathbf{c}_j; \theta^{(t+1)})}{Q^{(t)}(\mathbf{c}_j)} \\ &\geq \sum_{i=1}^N \sum_{j=1}^K Q^{(t)}(\mathbf{c}_j) \log \frac{p(\mathbf{x}_i, \mathbf{c}_j; \theta^{(t)})}{Q^{(t)}(\mathbf{c}_j)} = \ell(\theta^{(t)})\end{aligned}\quad (14)$$

The above result that $\ell(\theta^{(t)})$ monotonously increases with more iterations guarantees the convergence of the algorithm.

II Masked Intra-Sequence Contrastive Learning (MIC) as Expectation-Maximization

The proposed masked intra-sequence contrastive learning (MIC) can also be modeled as an Expectation-Maximization (EM) like algorithm, which is similar to the EM formulation in Sec. I. Specifically, the MIC implicitly involves two sets of variables, and solves two underlying sub-problems. The MIC loss function can be formulated as:

$$\mathcal{L}_{\text{MIC}}(\theta, \eta) = \mathbb{E}_{\mathbf{x}, \mathcal{M}} \left[\|f_{\theta}(\mathcal{M}(\mathbf{x})) - \eta_{\mathbf{x}}\|_2^2 \right], \quad (15)$$

where $f_{\theta}(\cdot)$ is the embedding/encoder function parameterized by θ . $\mathcal{M}(\cdot)$ is a random masking function, which could be viewed as an augmentation strategy to produce augmented instances (*i.e.*, subsequences) of the same skeleton sequence. For convenience, we simplify $\mathcal{M}(\cdot)$ with \mathbf{x} as the only input. \mathbf{x} is the input skeleton sequence. η denotes the set of variables related to representations of samples, and the subscript

\mathbf{x} means using the index of sample to access a sub-vector of η . Intuitively, $\eta_{\mathbf{x}}$ can be interpreted as the representation of the skeleton sequence \mathbf{x} . The expectation $\mathbb{E}[\cdot]$ is over the distribution of skeleton sequences and mask-based augmentation. The mean square error $\|\cdot\|_2^2$ is equivalent to the cosine similarity as the vectors are all ℓ_2 -normalized.

The objective of MIC is to minimize the mean square loss between the encoded representations of augmented skeleton instances and the representation of the skeleton instance. For the ease of analysis, we model MIC as an optimization problem by:

$$\min_{\theta, \eta} \mathcal{L}(\theta, \eta) \quad (16)$$

Analogous to the masked prototype contrastive learning (see Sec. I.1), the problem in formula (16) can be solved by an alternating algorithm. Formally, we can alternate between solving these two sub-problems:

$$\eta^{(t)} \leftarrow \arg \min_{\eta} \mathcal{L}(\theta^{(t)}, \eta), \quad (17)$$

$$\theta^{(t+1)} \leftarrow \arg \min_{\theta} \mathcal{L}(\theta, \eta^{(t)}), \quad (18)$$

where t is the index of alternation and \leftarrow denotes assigning.

In the t^{th} E-step (see Eq. (17)), the sub-problem is to minimize $\mathbb{E}_{\mathcal{M}} [\|f_{\theta^{(t)}}(\mathcal{M}(\mathbf{x})) - \eta_{\mathbf{x}}\|_2^2]$ for each skeleton sequence \mathbf{x} given the fixed $\theta^{(t)}$. Recalling the nature of the mean square error, it can be solved by:

$$\eta_{\mathbf{x}}^{(t)} \leftarrow \mathbb{E}_{\mathcal{M}} [f_{\theta^{(t)}}(\mathcal{M}(\mathbf{x}))], \quad (19)$$

where $\eta_{\mathbf{x}}$ is assigned with the average representation of \mathbf{x} over the distribution of mask-based augmentation.

For the t^{th} M-step (see Eq. (18)), the $\eta^{(t)}$ is naturally fixed as the gradient does not back-propagate to $\eta^{(t)}$, which is a constant in this sub-problem. We train model parameters θ to maximize the inherent similarity, *i.e.*, minimizing the mean square loss, between $f_{\theta}(\mathcal{M}(\mathbf{x}))$ and $\eta_{\mathbf{x}}^{(t)}$ get $\theta^{(t+1)}$.

II.1 Hypothesis for Effectiveness of Siamese Architectures

The proposed MIC can be approximated by one-step alternation between Eq. (17) and (18). In particular, we approximate Eq. (19) by sampling the mask-based augmentation only *once*, denoted as \mathcal{M}' , and ignoring $\mathbb{E}_{\mathcal{M}}[\cdot]$:

$$\eta_{\mathbf{x}}^{(t)} \leftarrow f_{\theta^{(t)}}(\mathcal{M}'(\mathbf{x})) \quad (20)$$

By inserting it into the sub-problem (see Eq. (18)) and combining Eq. (15), we can have:

$$\theta^{(t+1)} \leftarrow \arg \min_{\theta} \mathbb{E}_{\mathbf{x}, \mathcal{M}} \left[\|f_{\theta}(\mathcal{M}(\mathbf{x})) - f_{\theta^{(t)}}(\mathcal{M}'(\mathbf{x}))\|_2^2 \right], \quad (21)$$

where $\theta^{(t)}$ is a constant in this sub-problem, and \mathcal{M}' implies another random view generated by the proposed mask-based augmentation (*i.e.*, random subsequence sampling). The formulation in Eq. (21) exhibits a Siamese architecture naturally with stop-gradient applied, which leads to the hypothesis that the Siamese network matches the proposed EM modeling and is efficient for the optimization. This hypothesis is also theoretically and empirically proved in SimSiam [Chen and He, 2021].

II.2 Hypothesis for Effectiveness of Fully-Connected Layer

The predictor head attached on one side of the Siamese architecture is a commonly-adopted architecture in contrastive learning models [Chen *et al.*, 2020; Chen and He, 2021]. In our framework, we adopt a fully-connected (FC) layer (denoted as $\mathcal{F}_c(\cdot)$) rather than an MLP network as the predictor head. Here we hypothesize that \mathcal{F}_c is beneficial for the approximation of Eq. (20). Specifically, the predictor head $\mathcal{F}_c(\cdot)$ is expected to minimize $\mathbb{E}_{\mathbf{v}} [\|\mathcal{F}_c(\mathbf{v}_1) - \mathbf{v}_2\|_2^2]$, where $\mathbf{v}_1 = f_{\theta}(\mathcal{M}(\mathbf{x}_1))$, $\mathbf{v}_2 = f_{\theta}(\mathcal{M}(\mathbf{x}_2))$. Therefore, the optimal solution to \mathcal{F}_c should satisfy: $\mathcal{F}_c(\mathbf{v}_1) = \mathbb{E}_{\mathbf{v}}[\mathbf{v}_2] = \mathbb{E}_{\mathcal{M}}[f_{\theta}(\mathcal{M}(\mathbf{x}))]$ for any instance of skeleton sequence \mathbf{x} . This term is similar to the one in Eq. (19). Since the expectation $\mathbb{E}_{\mathcal{M}}$ is ignored in the approximation of Eq. (20), the hypothesis is that the application of $\mathcal{F}_c(\cdot)$ could fill this gap. Considering that directly computing the expectation $\mathbb{E}_{\mathcal{M}}$ is intractable and the masking function \mathcal{M} that samples random subsequences can be viewed as to linearly combine different skeletons of the same sequence, $\mathbb{E}_{\mathcal{M}}[f_{\theta}(\mathcal{M}(\mathbf{x}))]$ is assumed to be a linear transformation of skeleton features in the latent space (see our paper), thus we exploit a linear FC layer $\mathcal{F}_c(\cdot)$ to learn to predict the expectation, under the condition that the sampling of \mathcal{M} is implicitly distributed across multiple epochs. Theoretically, an MLP network is also feasible to approximate such expectation. In practice, using the FC layer or MLP can achieve similar performance on different datasets (see Appendix B), and the FC layer is adopted to enjoy smaller parameter size and lower computational complexity.

References

- [Chen and He, 2021] Xinlei Chen and Kaiming He. Exploring simple siamese representation learning. In *CVPR*, pages 15750–15758, 2021.
- [Chen *et al.*, 2020] Ting Chen, Simon Kornblith, Mohammad Norouzi, and Geoffrey Hinton. A simple framework for contrastive learning of visual representations. In *ICML*, 2020.
- [Ester *et al.*, 1996] Martin Ester, Hans-Peter Kriegel, Jörg Sander, Xiaowei Xu, et al. A density-based algorithm for discovering clusters in large spatial databases with noise. In *KDD*, volume 96, pages 226–231, 1996.
- [Gao *et al.*, 2021] Tianyu Gao, Xingcheng Yao, and Danqi Chen. Simcse: Simple contrastive learning of sentence embeddings. *arXiv preprint arXiv:2104.08821*, 2021.
- [He *et al.*, 2020] Kaiming He, Haoqi Fan, Yuxin Wu, Saining Xie, and Ross Girshick. Momentum contrast for unsupervised visual representation learning. In *CVPR*, pages 9729–9738, 2020.
- [Li *et al.*, 2021] Junnan Li, Pan Zhou, Caiming Xiong, and Steven Hoi. Prototypical contrastive learning of unsupervised representations. In *ICLR*, 2021.
- [Oord *et al.*, 2018] Aaron van den Oord, Yazhe Li, and Oriol Vinyals. Representation learning with contrastive predictive coding. *arXiv preprint arXiv:1807.03748*, 2018.
- [Wang and Isola, 2020] Tongzhou Wang and Phillip Isola. Understanding contrastive representation learning through alignment and uniformity on the hypersphere. In *ICML*, pages 9929–9939, 2020.

SimMC: Simple Masked Contrastive Learning of Skeleton Representations for Unsupervised Person Re-Identification - Appendix B Experiments

Haocong Rao and Chunyan Miao[†]

School of Computer Science and Engineering, Nanyang Technological University
Joint NTU-UBC Research Centre of Excellence in Active Living for the Elderly (LILY)
haocong001@ntu.edu.sg, ascymiao@ntu.edu.sg

I Supplementary Experimental Settings

In this section, we elaborate experimental settings including CASIA-B evaluation settings (Sec. I.1), dataset preprocessing (Sec. I.2), dataset probe settings (Sec. I.3) and framework implementation details (Sec. I.4).

I.1 Evaluation Settings for CASIA-B

It is noted that 3D skeleton data in existing skeleton-based person re-ID datasets are captured by Kinect [Shotton *et al.*, 2011]. To evaluate the effectiveness of our framework when 3D skeleton data are directly estimated from RGB videos rather than depth sensors such as Kinect, we introduce a large-scale RGB video based dataset, *CASIA-B* [Yu *et al.*, 2006], which contains walking sequences of 124 individuals under 11 different views and 3 conditions—pedestrians wearing a bag (“Bg”), wearing a coat (“CI”), and without any coat or bag (“Nm”). It should be noted that “B”, “C”, and “N” used in the paper denote “Bg”, “CI”, and “Nm”, respectively. We follow the evaluation setup in [Liu *et al.*, 2015], which is frequently used in the literature. We randomly leave half of IDs for training and use the rest for testing. All testing sequences are divided by three conditions (“Bg”, “CI”, “Nm”) to be gallery or probe sets, and we evaluate our approach under single-condition, *i.e.*, gallery set and probe set with the same condition, and cross-condition settings, *i.e.*, probe set is under normal condition (“Nm”) while gallery sets are under bag (“Bg”) or clothes condition (“CI”). Following [Liao *et al.*, 2020], we exploit pre-trained pose estimation models [Chen and Ramanan, 2017; Cao *et al.*, 2019] to extract 3D skeletons from RGB videos of CASIA-B. We first extract eighteen 2D joints from each person in videos by *OpenPose* model [Cao *et al.*, 2019]. Then, we follow the same configuration of estimation in [Liao *et al.*, 2020] and average the positions of “Nose”, “Reye”, “LEye”, “Rear” and “Lear” as the position of “Head” to construct fourteen 2D joints, which are fed into pose estimation method [Chen and Ramanan, 2017] to estimate corresponding 3D body joints. Thus, J is 14 for CASIA-B, and all joints in each skeleton are normalized by subtracting the neck joint.

Table 1: Statistics of different datasets. We construct different gallery and probe sets based on multiple testing splits (see Sec. I.3). For CASIA-B dataset, we exploit 3D skeleton data estimated from RGB videos (see Sec. I.1).

	KGBD	BIWI	KS20	IAS-Lab	CASIA-B
# Train IDs	164	50	20	11	124
# Train Skeletons	188,742	205,764	35,976	88,986	706,480
# Gallery IDs	164	28	20	11	62
# Gallery Skeletons	188,700	Walking: 4,932 Still: 3,186	3,252	IAS-A: 6,978 IAS-B: 7,764	Nm: 162,080 Cl: 54,400 Bg: 53,880
# Probe IDs	164	28	20	11	62
# Probe Skeletons	94,146	Walking: 4,932 Still: 3,186	3,306	IAS-A: 6,978 IAS-B: 7,764	Nm: 162,080 Cl: 54,400 Bg: 53,880

I.2 Dataset Preprocessing

To avoid ineffective skeleton recording, we discard the first and last 10 skeleton frames of each original skeleton sequence. For KS20, KGBD, BIWI, and IAS-Lab datasets, all skeleton sequences are normalized by subtracting the spine joint position from each joint of the same skeleton so that the skeleton is translation invariant [Zhao *et al.*, 2019]. Then, we split all normalized skeleton sequences in the training sets into multiple shorter skeleton sequences (*i.e.*, $S_{1:f}$) with length f by a step of $\frac{f}{2}$, which aims to obtain as many 3D skeleton sequences as possible to train our approach. We split all skeleton sequences in the gallery and probe sets into shorter and non-overlapped sequences with length f . Unless explicitly specified, the skeleton sequence $S_{1:f}$ in our paper refers to those split and normalized sequences used in learning, rather than those original skeleton sequences provided by datasets. We follow the data augmentation strategy used in [Rao *et al.*, 2021a; Rao *et al.*, 2021c] to sample more sequences for different classes in the training set, and train our framework with randomly shuffled and unlabeled skeleton sequences. The details of all datasets are shown in Table 1.

I.3 Dataset Probe Settings

For BIWI and IAS-Lab datasets, we set each testing set as the probe and the other one as the gallery. For KS20, we randomly select one skeleton sequence from each viewpoint as the probe sequence and use one half of the remaining se-

[†]Corresponding author

Table 2: Full results for performance comparison with appearance-based and skeleton-based methods on CASIA-B. “CI-Nm” represents the probe set under “Clothes” condition and gallery set under “Normal” condition. “—” indicates no published result.

Probe-Gallery	Nm-Nm			Bg-Bg			CI-CI			CI-Nm			Bg-Nm		
Methods	top-1	top-5	top-10 mAP	top-1	top-5	top-10 mAP	top-1	top-5	top-10 mAP	top-1	top-5	top-10 mAP	top-1	top-5	top-10 mAP
LMNN [Weinberger and Saul, 2009]	3.9	22.7	36.1	—	18.3	38.6	49.2	—	17.4	35.7	45.8	—	11.6	12.6	17.8
ITML [Davis <i>et al.</i> , 2007]	7.5	22.2	34.2	—	19.5	26.0	33.7	—	20.1	34.4	43.3	—	10.3	24.5	36.1
ELF [Gray and Tao, 2008]	12.3	35.6	50.3	—	5.8	25.5	37.6	—	19.9	43.9	56.7	—	5.6	16.0	26.3
SDALF [Farenzena <i>et al.</i> , 2010]	4.9	27.0	41.6	—	10.2	33.5	47.2	—	16.7	42.0	56.7	—	11.6	19.4	27.6
Score-based MLR [Liu <i>et al.</i> , 2015]	13.6	48.7	63.7	—	13.6	48.7	63.7	—	13.5	48.6	63.9	—	9.7	27.8	45.1
Feature-based MLR [Liu <i>et al.</i> , 2015]	16.3	43.4	60.8	—	18.9	44.8	59.4	—	25.4	53.3	68.9	—	20.3	42.6	56.9
AGE [Rao <i>et al.</i> , 2020]	20.8	29.3	34.2	3.5	37.1	56.2	67.0	9.8	35.5	54.3	65.3	9.6	14.6	33.0	42.7
SM-SGE [Rao <i>et al.</i> , 2021a]	50.2	73.5	81.9	6.6	26.6	49.0	59.4	9.3	27.2	51.4	63.2	9.7	10.6	26.3	35.9
SGELA [Rao <i>et al.</i> , 2021b]	71.8	87.5	91.4	9.8	48.1	69.5	77.7	16.5	51.2	73.8	81.5	7.1	15.9	30.8	40.6
SimMC (Ours)	84.8	92.3	93.7	10.8	69.1	86.6	91.3	16.5	68.0	88.1	93.0	15.7	25.6	43.8	54.0
													5.4	42.0	59.8
															68.9
															7.1

Table 3: The amount of network parameters (million (M)) and computational complexity (giga floating-point operations (GFLOPs)) of deep learning based methods. “+ DF” denotes direct supervised fine-tuning and “+ SimMC” represents unsupervised feature fine-tuning with the proposed SimMC framework. **Bold** refer to the smallest model size and computational complexity.

Types	Methods	# Params	GFLOPs
Supervised	PoseGait [Liao <i>et al.</i> , 2020]	8.93M	121.60
	SGELA [Rao <i>et al.</i> , 2021b] + DF	9.09M	7.48
	MG-SCR [Rao <i>et al.</i> , 2021c]	0.35M	6.60
	SM-SGE [Rao <i>et al.</i> , 2021a] + DF	6.25M	23.92
Self-supervised / Unsupervised	AGE [Rao <i>et al.</i> , 2020]	7.15M	37.37
	SGELA [Rao <i>et al.</i> , 2021b]	8.47M	7.47
	SM-SGE [Rao <i>et al.</i> , 2021a]	5.58M	22.61
	SimMC (Ours)	0.15M	0.99
Unsupervised Fine-tuning	SGELA + SimMC	8.80M	10.10
	MG-SCR + SimMC	0.53M	7.88
	SM-SGE + SimMC	5.89M	25.10

quences for training and the other half as the gallery. For KGBD, since no training and testing splits are given, we randomly leave one skeleton video of each person as the probe set, and equally divide the remaining videos into the training set and gallery set. For CASIA-B, we randomly leave half of IDs for training and use the rest for testing. All testing sequences are divided by three conditions, including Bag (Bg), Clothes (Cl), and Normal (Nm), to be gallery or probe sets, and we evaluate our framework under single-condition and cross-condition settings following [Liu *et al.*, 2015].

I.4 Implementation Details

All crucial experimental details are presented in our paper. The dimension of each input skeleton is $K = J \times 3$ as we concatenate all 3D coordinates of J body joints in order. The skeleton sequence length f on four skeleton-based datasets (IAS-Lab, KS20, BIWI, KGBD) is set to 6 following [Rao *et al.*, 2021b] for a fair comparison with existing methods. We empirically employ $x = 2$ random masks for subsequence sampling, which achieves best performance in average among different settings. As to CASIA-B, it is a large-scale dataset with roughly estimated skeleton data from RGB frames, which is intrinsically different from previous datasets. We adopt a longer sequence length $f = 40$, and empirically set $x = 10$ random masks for subsequence sampling in this dataset. The number of random subsequence sampling is $q = 2$ and the embedding size for skeleton representations is $H = 256$ for all datasets. It should be noted that we set

$q = 2$ to generate the instance (*i.e.*, subsequence representation) pair for the MIC scheme, while $q = 1$ is equivalent to $q = 2$ in the MPC scheme as the masking process is random. For DBSCAN clustering in the MPC scheme, we empirically set maximum distance $\epsilon = 0.6$ (KGBD, BIWI-S), $\epsilon = 0.8$ (KS20, IAS-Lab, BIWI-W), $\epsilon = 0.75$ (CASIA-B), and adopt minimum amount of samples $a_{min} = 4$ for KGBD and $a_{min} = 2$ for other datasets. We follow [Ge *et al.*, 2020; Dai *et al.*, 2021] to construct the commonly used Jaccard distance matrix to perform clustering, and discard all outliers in different clustered instance sets, *i.e.*, discard the union of all outliers, to perform contrastive learning. We set the temperature τ to 0.06 (KGBD), 0.075 (CASIA-B), 0.07 (BIWI), 0.08 (KS20, IAS-Lab) for MPC learning. The similarity weights α, β are equally set to 0.5 in the symmetrized MIC loss, while the weight coefficient λ is empirically set to 0.5 (IAS-B, KGBD, CASIA-B), 0.75 (IAS-A), and 0.25 (BIWI). We employ Adam optimizer with learning rate 0.00035 for all datasets. The batch size is set to 256 for all datasets. To avoid over-fitting and achieve better generalization performance, we adopt Early Stopping [Prechelt, 1998] with a patience of 100 epochs (*i.e.*, stop the training of model after no improvement in 100 continuous epochs). Interested readers can access our source codes* to get more details.

For all methods compared in our experiments, we select optimal model parameters for training, and use their pre-defined skeleton descriptors or pre-trained skeleton representations for person re-ID. It is worth noting that the performance of our re-implementation (*e.g.*, SGELA) is better than the original papers. For direct supervised fine-tuning (DF) of existing models, we attach an MLP network with one hidden layer to the end of original models, and train the MLP network on the frozen pre-trained representations with the supervision of labels. Then the feature representations before the last fully-connected layer are extracted for person re-ID. To perform unsupervised fine-tuning with SimMC, we train SimMC on the *unlabeled* and frozen skeleton representations pre-trained by original models, and exploit the skeleton representations learned by SimMC for person re-ID. Our framework is trained with only unlabeled skeleton data without using any post-processing technique, *e.g.*, re-ranking [Zhong *et al.*, 2017] or multi-query fusion [Zheng *et al.*, 2015]. To perform person re-ID, we exploit the framework to encode each original skeleton sequence without masking (*i.e.*,

*Our codes are available at <https://github.com/Kali-Hac/SimMC>.

Table 4: Performance of our framework on different datasets when setting different weight coefficients ($\lambda = 0.00, 0.25, 0.50, 0.75, 1.00$).

λ	KS20		KGBD		IAS-A		IAS-B		BIWI-W		BIWI-S	
	top-1	mAP	top-1	mAP	top-1	mAP	top-1	mAP	top-1	mAP	top-1	mAP
0.00	65.6	21.1	53.6	11.0	43.1	18.5	43.8	22.3	23.7	19.5	40.1	11.7
0.25	67.0	21.4	55.7	11.6	43.3	18.0	44.6	21.7	24.5	19.9	41.7	12.3
0.50	66.4	22.3	54.9	11.7	43.3	18.4	46.3	22.9	25.1	20.4	39.7	11.5
0.75	66.2	22.1	54.7	11.7	44.8	18.7	45.7	22.2	25.5	19.6	41.0	12.2
1.00	51.4	11.3	46.8	4.9	37.5	17.1	39.9	16.2	16.6	15.0	34.8	9.1

Table 5: Performance of our framework on different datasets when setting different numbers of masks ($x = 0, 1, 2, 3, 4$).

x	KS20		KGBD		IAS-A		IAS-B		BIWI-W		BIWI-S	
	top-1	mAP	top-1	mAP	top-1	mAP	top-1	mAP	top-1	mAP	top-1	mAP
0	65.8	20.8	54.3	10.9	40.2	17.3	40.6	21.3	23.4	18.7	39.8	11.6
1	66.2	20.7	54.9	11.0	43.8	18.2	43.7	21.5	23.6	20.1	41.5	12.2
2	66.4	22.3	54.9	11.7	44.8	18.7	46.3	22.9	24.5	19.9	41.7	12.3
3	66.6	21.6	54.9	11.3	44.3	17.8	44.8	22.1	24.9	18.8	41.0	12.1
4	63.9	22.0	54.7	12.0	42.4	17.1	41.3	17.3	20.7	16.8	41.2	11.7

$x = 0$) of the probe set Φ_P into corresponding representations, $\{\mathbf{v}_i^P\}_{i=1}^{N_2}$, and match it with representations, $\{\mathbf{v}_j^G\}_{j=1}^{N_3}$, of the same identity in the gallery set Φ_G using Euclidean distance. In ablation study, we use the concatenation of raw skeleton sequences (*i.e.*, normalized 3D coordinates of body joints) as the baseline.

II Supplementary Results

In this section, we provide full experimental results for model efficiency (Sec. II.1), CASIA-B evaluation (Sec. II.2), hyper-parameters (Sec. II.3, Sec. II.4, and Sec. II.5), training metrics (Sec. II.6), and confusion matrices (Sec. II.7).

II.1 Model Efficiency

We report the model efficiency in terms of model size, *i.e.*, amount of network parameters, and computational complexity for all deep learning based methods. For the model that possesses varying sizes and complexities on different datasets due to the changes of input data, we report the largest case. For models with direct supervised fine-tuning (“+ DF”) and unsupervised fine-tuning of SimMC (“+ SimMC”), we add the size of original models with the size of corresponding fine-tuning MLP network and the size of corresponding SimMC framework, respectively (Note that different output sizes of pre-trained skeleton representations influence the network size in fine-tuning process). As shown in Table 3, the proposed SimMC enjoys the smallest model size (only 0.15M) and GFLOPs[†] among all methods while achieving state-of-the-art performance in most cases (see our paper), which suggests its superior model efficiency for skeleton-based person re-ID tasks.

II.2 Evaluation with Model-Estimated Skeletons

To verify the effectiveness of our framework when using model-estimated 3D skeletons rather than Kinect-based

skeletons, we utilize pre-trained pose estimation models to extract 3D skeletons from RGB videos of CASIA-B, as detailed in Sec. I.1, and compare the performance of SimMC with representative appearance-based methods and state-of-the-art skeleton-based methods. It is worth noticing that the performance of our re-implementation (*e.g.*, SGELA) is better than the original papers. The full results are provided in Table 2. Due to the limitation of pages, we only compare the most representative appearance-based methods (ELF [Gray and Tao, 2008], SDALF [Farenzena *et al.*, 2010], Feature-based MLR [Liu *et al.*, 2015]) in our paper. As shown in Table 2, our framework can not only outperform state-of-the-art skeleton-based methods but also perform better than most classic appearance-based methods that utilize visual features (*e.g.*, colors, textures, and silhouettes) and extra label information, which suggests the great potential of SimMC to be applied to large RGB-based datasets under more general person re-ID settings.

II.3 Coefficient Settings for Contrastive Learning

We evaluate the performance of our framework with different weight coefficients ($\lambda = 0.00, 0.25, 0.50, 0.75, 1.00$) for combining MPC and MIC. As shown in Table 4, the proposed SimMC combining MPC and MIC achieves higher performance than solely employing MPC ($\lambda = 0.00$) or MIC ($\lambda = 1.00$). Since skeleton sequences of different datasets are typically captured or estimated in different conditions (*e.g.*, capturing frequency), the properties of sequences and their inherent relationships might be very different between two datasets, leading to a specific requirement of λ for masked intra-sequence contrastive learning. It can also be inferred that the MPC ($\lambda = 0.00$) contributes more than MIC ($\lambda = 1.00$) to the proposed SimMC, as using only MIC ($\lambda = 1.00$) cannot achieve satisfactory performance on all datasets, while incorporating them can maximize the performance gains. We employ $\lambda = 0.5$ for KS20, KGBD and IAS-B, $\lambda = 0.75$ for IAS-A, $\lambda = 0.25$ for BIWI-W and BIWI-S, which achieves the best performance among different settings.

[†]The GFLOPs here refer to computational complexity in the training of neural networks. Our model needs extra matrix computation in the clustering, where we employ Faiss library [Johnson *et al.*, 2019] to optimize the overall complexity.

Table 6: Performance of our framework on different datasets when setting different temperatures for the MPC scheme ($\tau = 0.06, 0.07, 0.08, 0.1, 0.5$).

τ	KS20		KGBD		IAS-A		IAS-B		BIWI-W		BIWI-S	
	top-1	mAP	top-1	mAP	top-1	mAP	top-1	mAP	top-1	mAP	top-1	mAP
0.06	67.4	21.8	54.9	11.7	44.1	18.6	46.3	21.8	25.1	20.9	41.6	11.9
0.07	66.6	22.2	55.1	12.1	44.8	18.5	47.3	22.2	24.5	19.9	41.7	12.3
0.08	66.4	22.3	55.9	12.4	44.8	18.7	46.3	22.9	24.6	19.8	41.8	10.7
0.1	65.8	21.8	55.3	11.8	44.0	18.3	47.5	23.8	24.1	19.5	41.4	11.2
0.5	67.6	21.4	55.4	12.1	43.9	18.7	48.6	25.1	24.7	19.6	42.0	11.5

Table 7: Performance of our framework on different datasets when setting different sequence length ($f = 2, 4, 6, 8$).

f	KS20		KGBD		IAS-A		IAS-B		BIWI-W		BIWI-S	
	top-1	mAP	top-1	mAP	top-1	mAP	top-1	mAP	top-1	mAP	top-1	mAP
4	62.6	19.0	53.9	10.9	43.2	19.2	46.5	20.5	21.2	16.9	38.4	11.1
6	66.4	22.3	54.9	11.7	44.8	18.7	46.3	22.9	24.5	19.9	41.7	12.3
8	69.9	28.0	55.9	12.9	44.4	24.1	47.7	26.7	24.4	27.6	42.6	14.9
10	69.5	24.8	55.5	12.3	43.2	19.5	44.2	30.0	28.9	23.1	37.7	16.5

II.4 Mask Settings for Subsequence Sampling

We evaluate the performance of SimMC when setting different numbers of masks ($x = 0, 1, 2, 3, 4$) for sampling random subsequences. As shown in Table 5, applying masked contrastive learning ($x > 0$) can encourage the model to learn better skeleton representations and achieve higher performance in average than directly performing contrastive learning with original sequences ($x = 0$) and MIC. However, too many masks (*e.g.*, $x > 3$) could hurt the overall model performance on all datasets. Considering that the sequence length of the original sequence is 6, when $x > 3$, more than half of the skeleton sequence and corresponding pattern information are masked and discarded in the training, which could result in a large loss of valuable skeleton features in clustering/contrastive learning and negatively influence the quality of learned skeleton representations for person re-ID. In our framework, we empirically set a relatively small value $x = 2$ for all datasets.

II.5 Other Hyper-Parameters

Temperature Setting for Contrastive Learning

As shown in Table 6, our framework is not sensitive to the changes of temperatures and can achieve comparable performance in the range of 0.06 to 0.5. In practice, we empirically select an appropriate temperature for each dataset to achieve more balanced and better model performance.

Different Sequence Lengths

We provide the performance results of our framework when using different sequence length ($f = 4, 6, 8, 10$) in Table 7. In our paper, we evaluate all compared methods under the same sequence length ($f = 6$).

Different Embedding Sizes

We evaluate the performance of SimMC when using different embedding sizes ($H = 64, 128, 256, 512$) in Table 8. Too small embedding size ($H = 64$) is shown to obtain lower performance in most cases, while larger sizes ($H > 256$) cannot further improve the performance. This suggests that too high-dimensional feature space might be hard to optimize

and contain more redundant information, which cannot benefit learning a compact and effective representation.

Different Settings for DBSCAN

We provide the performance results of our framework when setting different minimum sample amounts ($a_{min} = 1, 2, 3, 4$) and maximum distances ($\epsilon = 0.4, 0.6, 0.8, 1.0$) in Table 9 and Table 10, respectively. Note that we adjust a specific parameter while keeping other parameters unchanged, as illustrated in Sec. I.4. Our framework is robust to the change of a_{min} , while it is more sensitive to the parameter ϵ . Too high ϵ (*e.g.*, $\epsilon = 1.0$) is shown to reduce the overall performance on five of six testing sets (KGBD, IAS-A, IAS-B, BIWI-W, BIWI-S), while adopting relatively small ϵ (*e.g.*, $\epsilon = 0.6$), *i.e.*, reducing the connectedness of skeleton instances in clusters and improving the amount of prototypes, can facilitate person re-ID performance in most cases. Such results suggest that performing masked contrastive learning with more diverse skeleton prototypes could encourage mining richer discriminative features from unlabeled skeletons of different datasets.

Different Hidden Layers and Predictor Heads

We show the performance of our framework when exploiting the MLP encoder with different numbers of hidden layers (1, 2, 3, 4) in Table 11. It is observed that the addition of hidden layers does not bring extra performance gains to our framework, and it could even lead to an evident performance degradation. Different from [Chen and He, 2021] that employs two hidden layers with up to 2048-d embedding size to learn large-scale image data, our framework can learn better skeleton representations with simpler network structure on relatively limited training data (Note that ImageNet data used in [Chen and He, 2021] are much larger than skeleton data and require deeper neural networks to sufficiently learn patterns). Based on this observation, we exploit the MLP encoder with one hidden layer for masked contrastive learning. Likewise, in the Siamese architecture of MIC, we construct a simpler predictor head with fully-connected (FC) layer instead of MLP (see hypotheses and proof in Appendix A). As shown in Table 12, the predictor head using FC or MLP

Table 8: Performance of our framework on different datasets when setting different embedding sizes for skeleton representations ($H = 64, 128, 256, 512$).

	KS20		KGBD		IAS-A		IAS-B		BIWI-W		BIWI-S	
H	top-1	mAP	top-1	mAP	top-1	mAP	top-1	mAP	top-1	mAP	top-1	mAP
64	65.4	20.7	51.8	11.2	44.6	18.5	46.7	22.1	15.9	15.9	42.1	12.6
128	67.0	19.8	53.6	11.4	43.7	18.8	47.3	23.2	25.0	20.4	43.0	11.3
256	66.4	22.3	54.9	11.7	44.8	18.7	46.3	22.9	24.5	19.9	41.7	12.3
512	66.2	22.1	56.0	12.1	43.5	18.8	46.5	23.1	25.0	20.6	41.6	11.8

Table 9: Performance of our framework on different datasets when setting different minimum amounts of samples for the DBSCAN algorithm ($a_{min} = 1, 2, 3, 4$).

	KS20		KGBD		IAS-A		IAS-B		BIWI-W		BIWI-S	
a_{min}	top-1	mAP	top-1	mAP	top-1	mAP	top-1	mAP	top-1	mAP	top-1	mAP
1	66.3	22.4	56.4	11.4	43.0	18.7	46.6	22.5	24.7	19.8	41.6	12.0
2	66.4	22.3	55.8	11.7	44.8	18.7	46.3	22.9	24.5	19.9	41.7	12.3
3	67.4	22.3	54.7	11.9	44.4	18.3	47.9	22.9	24.6	19.9	42.2	11.6
4	65.6	21.3	54.9	11.7	44.8	19.9	47.0	23.7	25.4	20.4	42.6	12.3

can achieve highly similar performance on different datasets, while FC can enjoy lower complexity than MLP to construct more efficient framework.

II.6 Visualization of Training Process

We visualize the total training loss, MPC training loss, and MIC training losses in Fig. 1, Fig. 2, and Fig. 3 respectively, which show that the training of our framework can converge very fast in the first 50 optimization epochs. To provide a further analysis of the learned skeleton representations, we follow the method in [Ross, 2014] to estimate the mutual information between the skeleton instance features and the ground-truth class labels, as shown in Fig. 4. The results show that the training of our framework rapidly and significantly improves the mutual information *w.r.t.* skeleton representations, *i.e.*, similarity between the pseudo classes generated by SimMC and ground-truth class labels, which demonstrates that the proposed masked contrastive learning can encourage the model to capture class-related semantics (*e.g.*, inter-class differences) to learn more discriminative skeleton representations. Besides, we evaluate the uniformity of the representation distributions on the output unit hypersphere, which is one of the key properties related to contrastive learning and can indicate the quality of learned features. We follow [Wang and Isola, 2020] to compute the uniform loss in the training process, as shown in Fig. 5. It is seen that the training of SimMC evidently improves the feature uniformity (*i.e.*, lower uniform loss) on different datasets, which suggests that the proposed masked contrastive learning could effectively mine more useful features and enhance the expressiveness of skeleton representations to [Gao *et al.*, 2021].

II.7 Confusion Matrix Visualization

In Fig. 6, we show the confusion matrices of our framework when performing person re-ID with the top-1 matching (*i.e.*, predict the identity using the representation with the smallest Euclidean distance) on all testing sets (probes).

References

- [Cao *et al.*, 2019] Zhe Cao, Gines Hidalgo, Tomas Simon, Shih-En Wei, and Yaser Sheikh. Openpose: realtime multi-person 2d pose estimation using part affinity fields. *IEEE transactions on pattern analysis and machine intelligence*, 43(1):172–186, 2019.
- [Chen and He, 2021] Xinlei Chen and Kaiming He. Exploring simple siamese representation learning. In *CVPR*, pages 15750–15758, 2021.
- [Chen and Ramanan, 2017] Ching-Hang Chen and Deva Ramanan. 3d human pose estimation= 2d pose estimation+ matching. In *CVPR*, pages 7035–7043, 2017.
- [Dai *et al.*, 2021] Zuozhuo Dai, Guangyuan Wang, Weihao Yuan, Siyu Zhu, and Ping Tan. Cluster contrast for unsupervised person re-identification. *arXiv preprint arXiv:2103.11568*, 2021.
- [Davis *et al.*, 2007] Jason V Davis, Brian Kulis, Prateek Jain, Suvrit Sra, and Inderjit S Dhillon. Information-theoretic metric learning. In *ICML*, pages 209–216, 2007.
- [Farenzena *et al.*, 2010] Michela Farenzena, Loris Bazzani, Alessandro Perina, Vittorio Murino, and Marco Cristani. Person re-identification by symmetry-driven accumulation of local features. In *CVPR*, pages 2360–2367. IEEE, 2010.
- [Gao *et al.*, 2021] Tianyu Gao, Xingcheng Yao, and Danqi Chen. Simcse: Simple contrastive learning of sentence embeddings. *arXiv preprint arXiv:2104.08821*, 2021.
- [Ge *et al.*, 2020] Yixiao Ge, Feng Zhu, Dapeng Chen, Rui Zhao, and Hongsheng Li. Self-paced contrastive learning with hybrid memory for domain adaptive object re-id. In *NeurIPS*, 2020.
- [Gray and Tao, 2008] Douglas Gray and Hai Tao. Viewpoint invariant pedestrian recognition with an ensemble of localized features. In *ECCV*, pages 262–275. Springer, 2008.
- [Johnson *et al.*, 2019] Jeff Johnson, Matthijs Douze, and Hervé Jégou. Billion-scale similarity search with gpus. *IEEE Transactions on Big Data*, 2019.

Table 10: Performance of our framework on different datasets when setting different maximum distances ($\epsilon = 0.4, 0.6, 0.8, 1.0$).

ϵ	KS20		KGBD		IAS-A		IAS-B		BIWI-W		BIWI-S	
	top-1	mAP	top-1	mAP	top-1	mAP	top-1	mAP	top-1	mAP	top-1	mAP
0.4	65.8	22.9	52.1	9.2	44.5	20.2	47.4	25.6	17.5	16.3	39.8	11.2
0.6	67.0	22.5	54.9	11.7	43.3	19.6	46.2	23.7	23.2	18.5	41.7	12.3
0.8	66.4	22.3	48.5	5.3	44.8	18.7	46.3	22.9	24.5	19.9	40.5	12.1
1.0	66.8	21.6	44.6	5.0	42.6	18.5	43.6	22.3	20.2	17.3	24.8	7.1

Table 11: Performance of our framework on different datasets when setting different numbers of hidden layers for the MLP encoder.

Hidden Layers	KS20		KGBD		IAS-A		IAS-B		BIWI-W		BIWI-S	
	top-1	mAP	top-1	mAP	top-1	mAP	top-1	mAP	top-1	mAP	top-1	mAP
1	66.4	22.3	54.9	11.7	44.8	18.7	46.3	22.9	24.5	19.9	41.7	12.3
2	64.8	21.4	52.2	11.0	41.6	18.8	46.2	23.0	23.2	18.9	40.4	11.6
3	64.7	21.7	48.4	9.9	40.4	18.1	42.8	22.3	22.8	19.5	38.3	12.0
4	62.7	22.0	46.2	9.3	39.8	18.9	40.9	22.7	19.5	15.6	34.2	12.6

- [Liao *et al.*, 2020] Rijun Liao, Shiqi Yu, Weizhi An, and Yongzhen Huang. A model-based gait recognition method with body pose and human prior knowledge. *Pattern Recognition*, 98:107069, 2020.
- [Liu *et al.*, 2015] Zheng Liu, Zhaoxiang Zhang, Qiang Wu, and Yunhong Wang. Enhancing person re-identification by integrating gait biometric. *Neurocomputing*, 168:1144–1156, 2015.
- [Prechelt, 1998] Lutz Prechelt. Early stopping-but when? In *NeurIPS workshop*, pages 55–69, 1998.
- [Rao *et al.*, 2020] Haocong Rao, Siqi Wang, Xiping Hu, Mingkui Tan, Huang Da, Jun Cheng, and Bin Hu. Self-supervised gait encoding with locality-aware attention for person re-identification. In *IJCAI*, volume 1, pages 898–905, 2020.
- [Rao *et al.*, 2021a] Haocong Rao, Xiping Hu, Jun Cheng, and Bin Hu. Sm-sge: A self-supervised multi-scale skeleton graph encoding framework for person re-identification. In *Proceedings of the 29th ACM international conference on Multimedia*, 2021.
- [Rao *et al.*, 2021b] Haocong Rao, Siqi Wang, Xiping Hu, Mingkui Tan, Yi Guo, Jun Cheng, Xinwang Liu, and Bin Hu. A self-supervised gait encoding approach with locality-awareness for 3d skeleton based person re-identification. *IEEE Transactions on Pattern Analysis and Machine Intelligence*, 2021.
- [Rao *et al.*, 2021c] Haocong Rao, Shihao Xu, Xiping Hu, Jun Cheng, and Bin Hu. Multi-level graph encoding with structural-collaborative relation learning for skeleton-based person re-identification. In *IJCAI*, 2021.
- [Ross, 2014] Brian C Ross. Mutual information between discrete and continuous data sets. *PloS one*, 9(2):e87357, 2014.
- [Shotton *et al.*, 2011] Jamie Shotton, Andrew Fitzgibbon, Mat Cook, Toby Sharp, Mark J Finocchio, Richard Moore, Alex Abenathar Kipman, and Andrew Blake. Real-time human pose recognition in parts from single depth images. In *CVPR*, pages 1297–1304, 2011.
- [Wang and Isola, 2020] Tongzhou Wang and Phillip Isola. Understanding contrastive representation learning through alignment and uniformity on the hypersphere. In *ICML*, pages 9929–9939, 2020.
- [Weinberger and Saul, 2009] Kilian Q Weinberger and Lawrence K Saul. Distance metric learning for large margin nearest neighbor classification. *Journal of machine learning research*, 10(2), 2009.
- [Yu *et al.*, 2006] Shiqi Yu, Daoliang Tan, and Tieniu Tan. A framework for evaluating the effect of view angle, clothing and carrying condition on gait recognition. In *ICPR*, volume 4, pages 441–444. IEEE, 2006.
- [Zhao *et al.*, 2019] Rui Zhao, Kang Wang, Hui Su, and Qiang Ji. Bayesian graph convolution lstm for skeleton based action recognition. In *ICCV*, pages 6882–6892, 2019.
- [Zheng *et al.*, 2015] Liang Zheng, Liye Shen, Lu Tian, Shengjin Wang, Jingdong Wang, and Qi Tian. Scalable person re-identification: A benchmark. In *ICCV*, pages 1116–1124, 2015.
- [Zhong *et al.*, 2017] Zhun Zhong, Liang Zheng, Donglin Cao, and Shaozi Li. Re-ranking person re-identification with k-reciprocal encoding. In *CVPR*, pages 1318–1327, 2017.

Table 12: Performance of our framework on different datasets when adopting different types of predictor head (fully-connected layer (FC) or multi-layer perceptron (MLP)).

	KS20		KGBD		IAS-A		IAS-B		BIWI-W		BIWI-S	
Predictor Head	top-1	mAP	top-1	mAP	top-1	mAP	top-1	mAP	top-1	mAP	top-1	mAP
FC	66.4	22.3	54.9	11.7	44.8	18.7	46.3	22.9	24.5	19.9	41.7	12.3
MLP	66.6	21.9	55.8	11.2	44.7	19.1	48.1	24.9	24.6	20.7	42.7	11.9

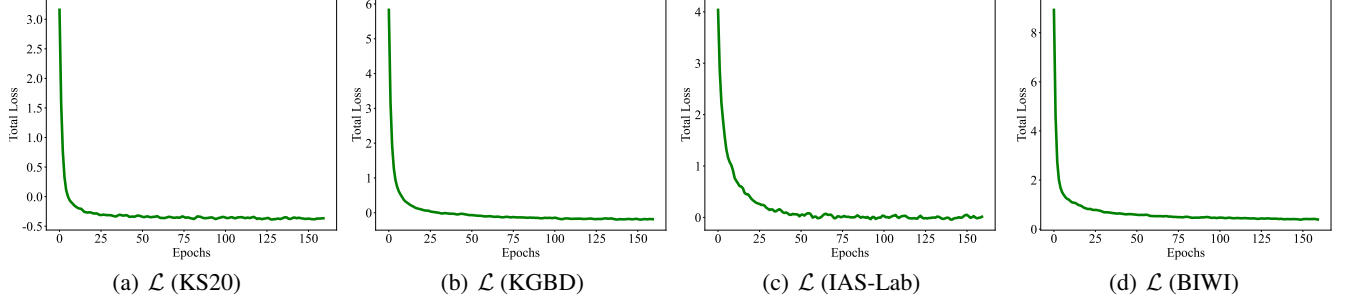


Figure 1: Total masked contrastive learning loss ($\mathcal{L} = \lambda\mathcal{L}_{\text{MIC}} + (1 - \lambda)\mathcal{L}_{\text{MPC}}$) curves on the training sets of different datasets.

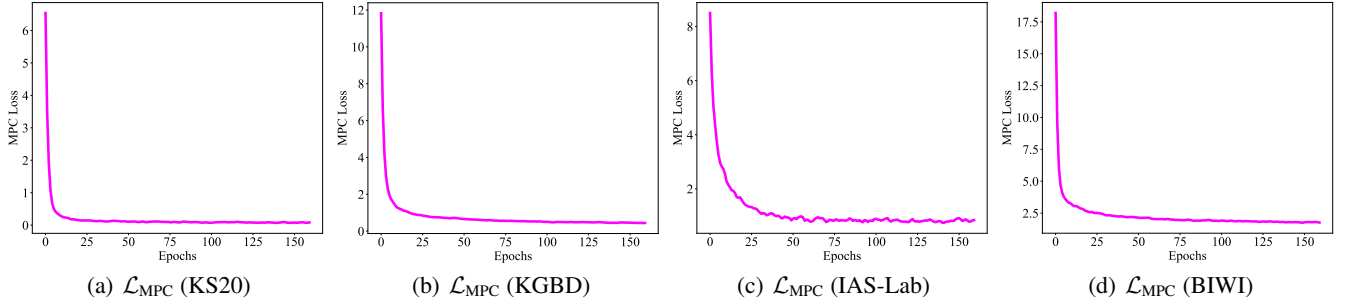


Figure 2: Masked prototype contrastive (MPC) loss (\mathcal{L}_{MPC}) curves on the training sets of different datasets.

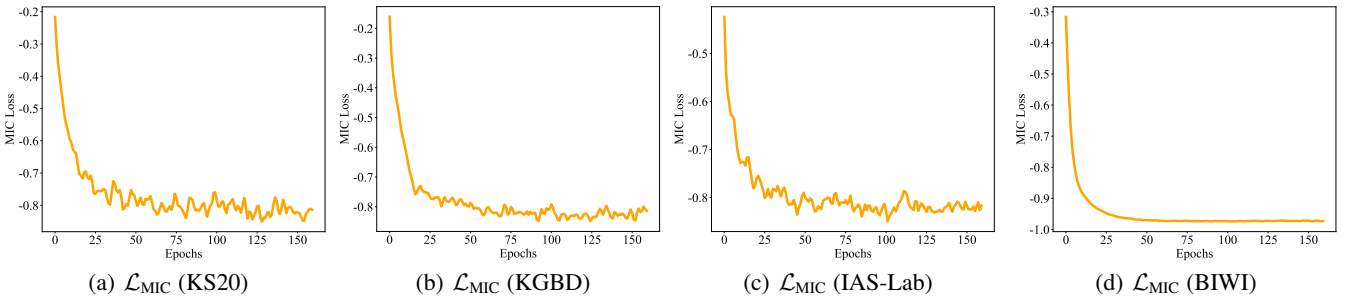


Figure 3: Masked intra-sequence contrastive (MIC) loss (\mathcal{L}_{MIC}) curves on the training sets of different datasets.

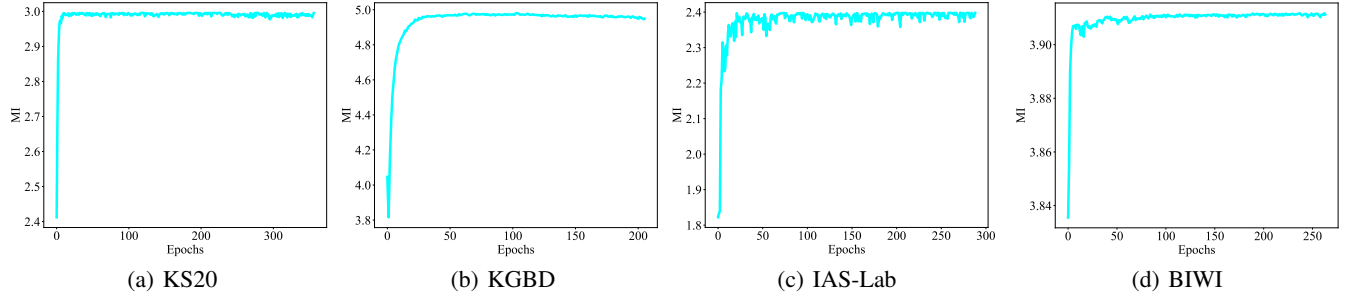


Figure 4: Mutual information (MI) between the clusters/pseudo classes generated by SimMC and ground-truth class labels on the training sets of different datasets.

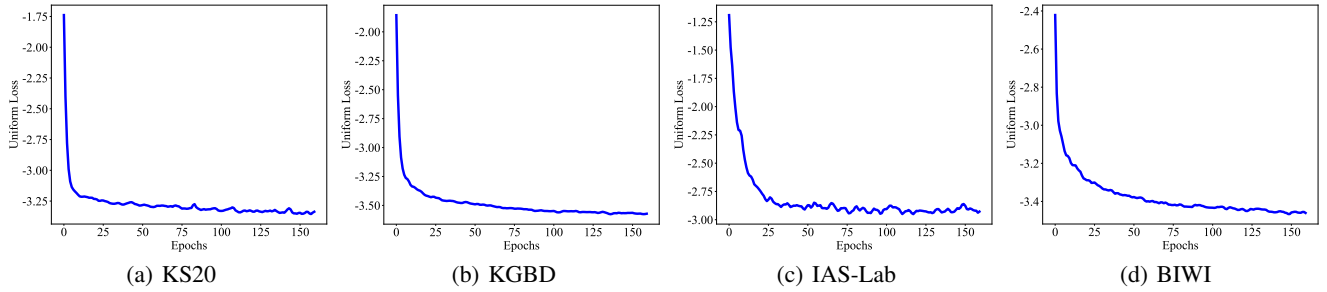
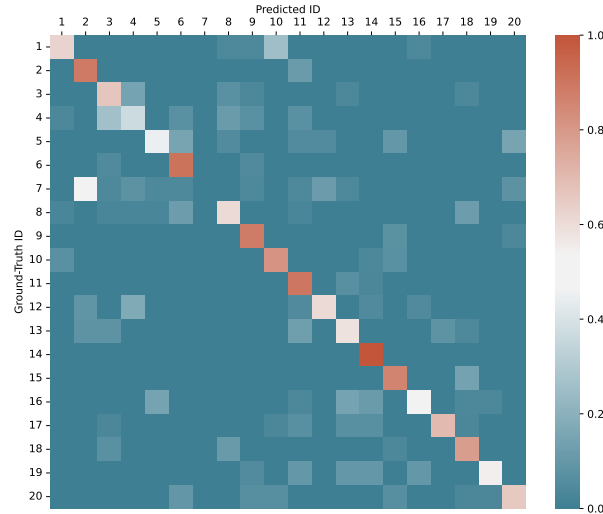
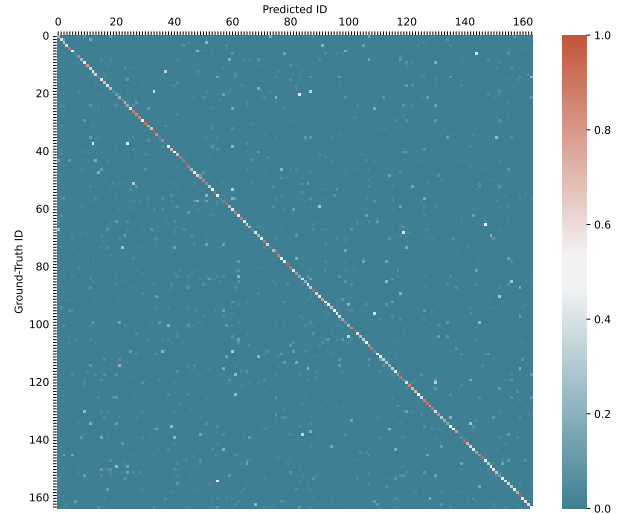


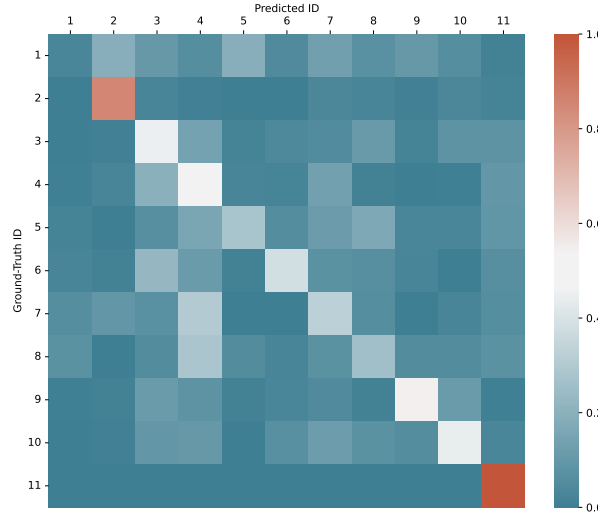
Figure 5: Uniform loss curves on the training sets of different datasets. Lower uniform loss indicates higher uniformity of feature distributions on the output unit hypersphere, which could suggest the higher quality of the learned representations (see Sec. II.6).



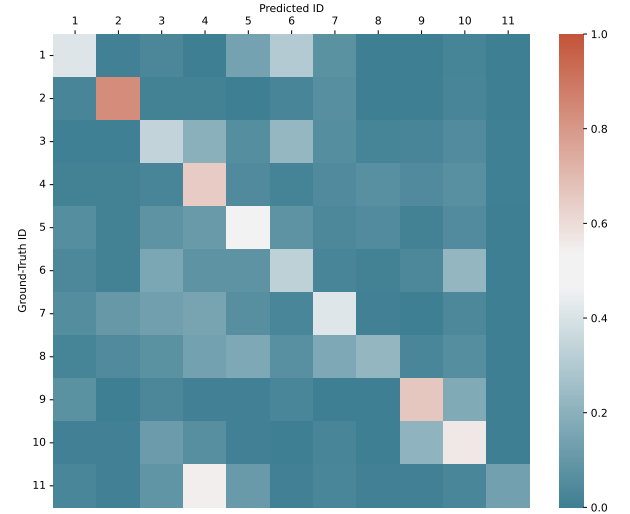
(a) Confusion Matrix on KS20



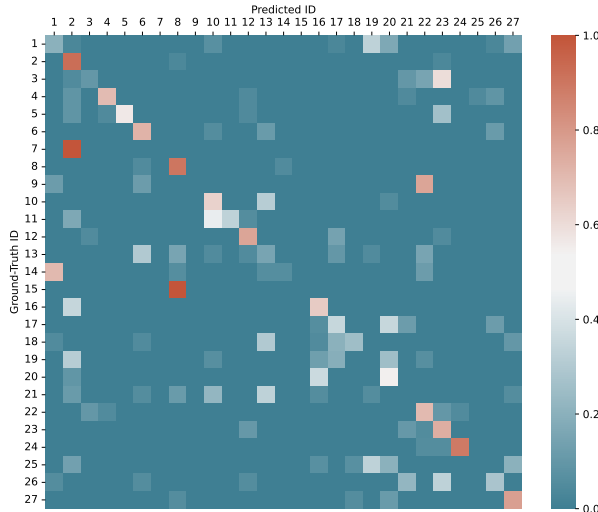
(b) Confusion Matrix on KGBD



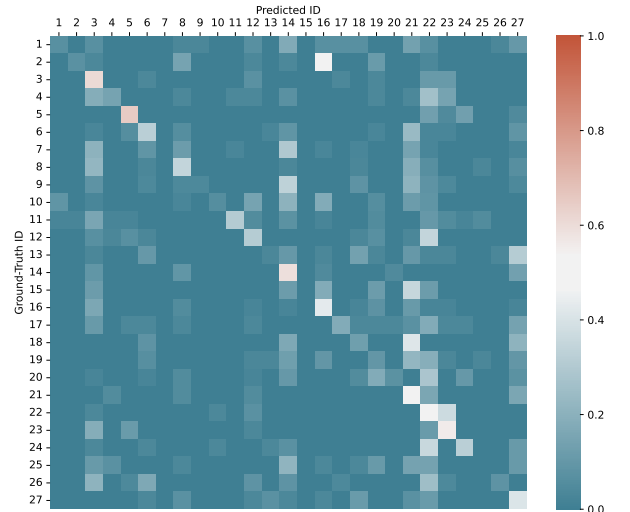
(c) Confusion Matrix on IAS-A



(d) Confusion Matrix on IAS-B



(e) Confusion Matrix on BIWI-Still



(f) Confusion Matrix on BIWI-Walking

Figure 6: Visualization of confusion matrices on KS20 (a), KGBD (b), IAS-A (c), IAS-B (d), BIWI-Still (e), and BIWI-Walking (f) when using the top-1 matching. Note that abscissa and ordinate denote the predicted and ground-truth identities, respectively. The position in the a^{th} row and b^{th} column indicates that the testing samples belonging to the a^{th} identity is predicted as the b^{th} identity, while the corresponding value is the proportion of such samples to the same-class samples in the testing set.